


REVIEW

Open Access



# Thermal photonics with broken symmetries

Tianji Liu<sup>1†</sup>, Cheng Guo<sup>2†</sup>, Wei Li<sup>1\*</sup>  and Shanhui Fan<sup>3\*</sup>

## Abstract

Nanophotonic engineering provides an effective platform to manipulate thermal emission on-demand, enabling unprecedented heat management superior to conventional bulk materials. Amongst a plethora of nanophotonic structures, symmetries play an important role in controlling radiative heat transfer in both near-field and far-field. In physics, broken symmetries generally increase the degree of freedom in a system, enriching the understanding of physical mechanisms and bringing many exciting opportunities for novel applications. In this review, we discussed the underlying physics and functionalities of nanophotonic structures with broken geometrical symmetries, engineered mode symmetries, and broken reciprocity for the control of thermal emission. We overview a variety of physical phenomena and interesting applications, and provide the outlook for future development.

## 1 Introduction

Radiative heat transfer is a ubiquitous physical process in our universe. Any object with a temperature above absolute zero exchanges thermal energy with the environment. In physics, thermal emission originates from electromagnetic radiation induced by the thermal motion of charged particles inside materials. Planck's law characterizes the spectral distribution of emitted power. The second law of thermodynamics governs the irreversibility of energy transfer in thermal emission. In conventional systems, thermal emission tends to be broadband, incoherent, omnidirectional, and unpolarized, due to fluctuating electromagnetic fields thermally generated inside materials. Thanks to the rapid development of nanophotonics, researchers demonstrated that thermal emission, similar to spontaneous emission of light, can be engineered or manipulated with the use of artificial or naturally occurring micro/nanostructures [1]. Narrowband, directional, or polarized thermal emissions are all

proposed and experimentally demonstrated using metamaterials [2, 3]. Fruitful achievements propel the development of thermal photonics which improves energy utilization efficiency and revolutionizes many energy applications. Several review papers have comprehensively overviewed the field of thermal photonics, specifically the radiative heat transfer in near-field and far-field [2–7].

Symmetries are of fundamental importance in physics [8]. A symmetry of a physical system is a physical feature that remains invariant under some transformation. The transformations may be continuous or discrete, which give rise to the corresponding types of symmetries. Symmetries are mathematically described by groups. Continuous symmetries are described by Lie groups while discrete symmetries are described by finite groups. The continuous symmetries of a physical system are intimately related to the conservation laws characterizing that system. For example, the temporal translation symmetry gives rise to the conservation of energy.

Symmetries also play an important role in thermal radiation [9, 10]. In this context, the relevant symmetries include the geometric and non-geometric ones. The geometric symmetries refer to the invariance of the system, including both the thermal emitter and its environment, under the usual spatial transformation such as rotation, reflection, and inversion. The non-geometric symmetries include reciprocity, energy

<sup>†</sup>Tianji Liu and Cheng Guo contributed equally to this work

\*Correspondence: weilil1@ciomp.ac.cn; shanhui@stanford.edu

<sup>1</sup> GPL Photonics Laboratory, State Key Laboratory of Applied Optics, Fine Mechanics and Physics, Changchun Institute of Optics, Chinese Academy of Sciences, Changchun 130033, China

<sup>3</sup> Department of Electrical Engineering, Ginzton Laboratory, Stanford University, Stanford, CA 94305, USA

Full list of author information is available at the end of the article

conservation, and time-reversal symmetry, which are invariance under the corresponding internal transformations of linear photonic systems [9].

These symmetries have important implications for thermal radiation. For example, any thermal emitter is fundamentally characterized by two key quantities: the angular spectral absorptivity  $\alpha(\omega, -\hat{n}, \hat{p})$  and the angular spectral emissivity  $e(\omega, \hat{n}, \hat{p})$  [10].  $\alpha(\omega, -\hat{n}, \hat{p})$  represents the absorption coefficient for incident light at frequency  $\omega$  and direction  $-\hat{n}$  with a complex polarization vector  $\hat{p}$ .  $e(\omega, \hat{n}, \hat{p})$  measures the spectral emission power per unit area at the frequency  $\omega$  in the direction  $\hat{n}$  with a polarization  $\hat{p}$ , normalized against a blackbody at the same temperature as the emitter. It is known that the existence of geometric and non-geometric symmetries imposes direct constraints on  $\alpha(\omega, -\hat{n}, \hat{p})$  and  $e(\omega, \hat{n}, \hat{p})$ . Conversely, breaking these symmetries can remove such constraints. As a simple but important example, we note that any linear time-invariant thermal emitter needs be lossy, and thus must break energy

conservation and time-reversal symmetry [9]; however, it can either obey or violate Lorentz reciprocity.

In this review, we will examine the important physical consequences of symmetry breaking on thermal radiation, as shown in Fig. 1, in contrast to general thermal photonic structures or structures with high symmetry [11–14]. We will schematically illustrate the physical mechanisms and practical applications for each type of reduced symmetries. The review is organized as follows: Section "Breaking geometric symmetries" reviews metastructures with broken geometric symmetries. In Section "Anisotropy", we review anisotropic metastructures with in-plane or out-of-plane anisotropy. In Section "Aperiodicity and randomness", we discuss aperiodic or random structures that break translational symmetry. These structures allow for extra freedom in photonic design and more cost-effective and large-area fabrications. In Section "Chirality", we examine chiral metastructures for thermal photonic applications. We discuss circularly polarized thermal emission, optical Rashba effect, photothermal circular dichroism,

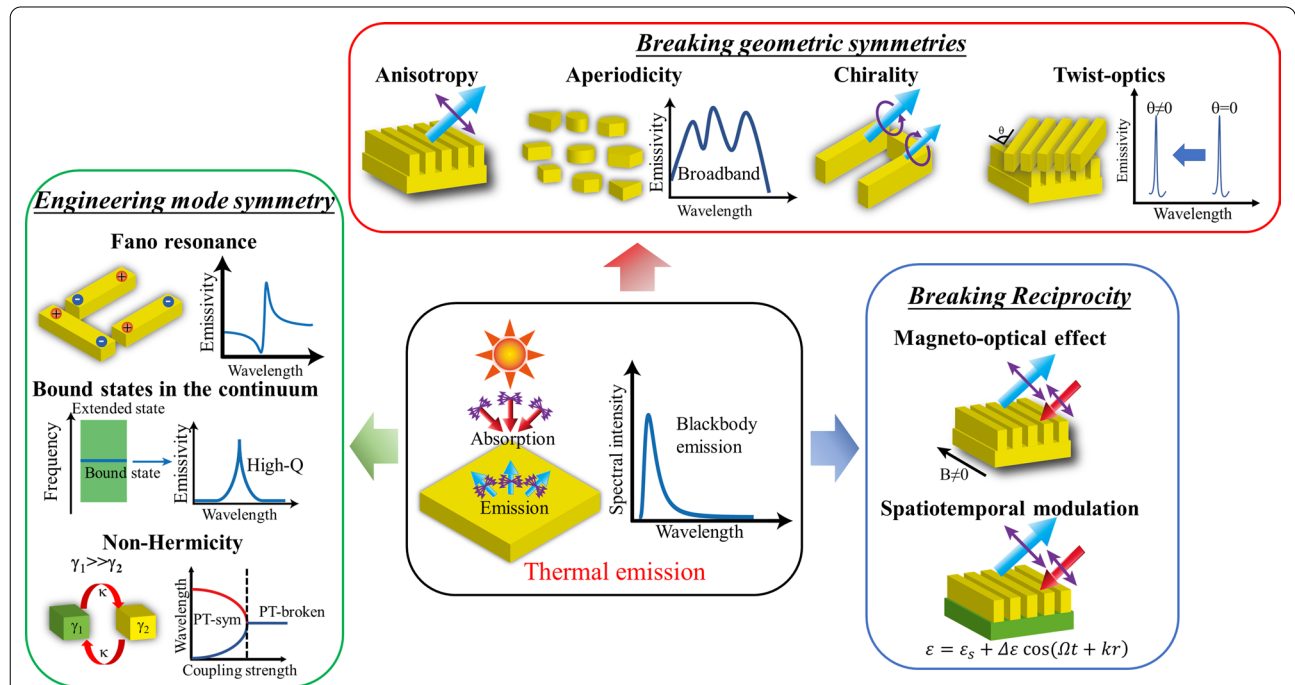


**Fig. 1** Thermal photonics with broken symmetries. Without nanophotonic engineering (central panel), the general thermal emission exhibits omnidirectional, incoherent, unpolarized, and reciprocal features. The spectral density of an ideal thermal emitter with unity emissivity can be described by Planck’s law of blackbody emission. With broken geometrical symmetries (top panel), using anisotropic metastructures can tailor emission angle and polarization; Aperiodic or randomized structures may expand the emission band; Chiral structures show differential responses for circularly polarized thermal emission; Twist-optical metastructures are responsible for twist-angle sensitive narrow band thermal emission. With engineered mode symmetries (left panel), Fano resonance, bound states in the continuum, and non-Hermitian at the exceptional point can be formed as peculiar optical states. The mode symmetries play an important role in the formation of each optical state, enabling unconventional thermal emission control such as asymmetric spectral line-shape of emissivity, ultrahigh quality factor, and the transition of emissivity near the exceptional point, respectively. To break reciprocity (lower right panel), magneto-optical materials and spatiotemporal modulation can be exploited for nonreciprocal thermal emission control, indicating the ability to violate Kirchhoff’s law of thermal radiation

and thermal nonequilibrium generated spin angular momenta. Section "Engineering mode symmetries" reviews metastructures with engineered mode symmetry. In Section "Fano resonance", we discuss Fano resonances. In Section "Bound states in the continuum (BIC)", we discuss bound states in the continuum. We cover thermal applications of such modes, including wavelength-selective and narrowband near-field radiative heat transfer, and complete on-off switching of thermal emission. Section "Breaking reciprocity" reviews metastructures that break reciprocity. In Section "Magneto-optical effect", we discuss nonreciprocal thermal effects based on magneto-optical materials, such as violation of Kirchhoff's law of thermal radiation, persistent directional heat current, and photon thermal Hall effect. In Section "Spatiotemporal modulation", we discuss nonreciprocal thermal effects based on space-time modulation. Section "Summary and outlook" briefly discusses several emerging research directions in thermal photonics. In Section "Non-Hermiticity", we discuss non-Hermitian systems with or without parity-time symmetry, which may exhibit exceptional points. In Section "Twist-optics", we discuss twist-optical

systems, which may enable great tunability of thermal emission.

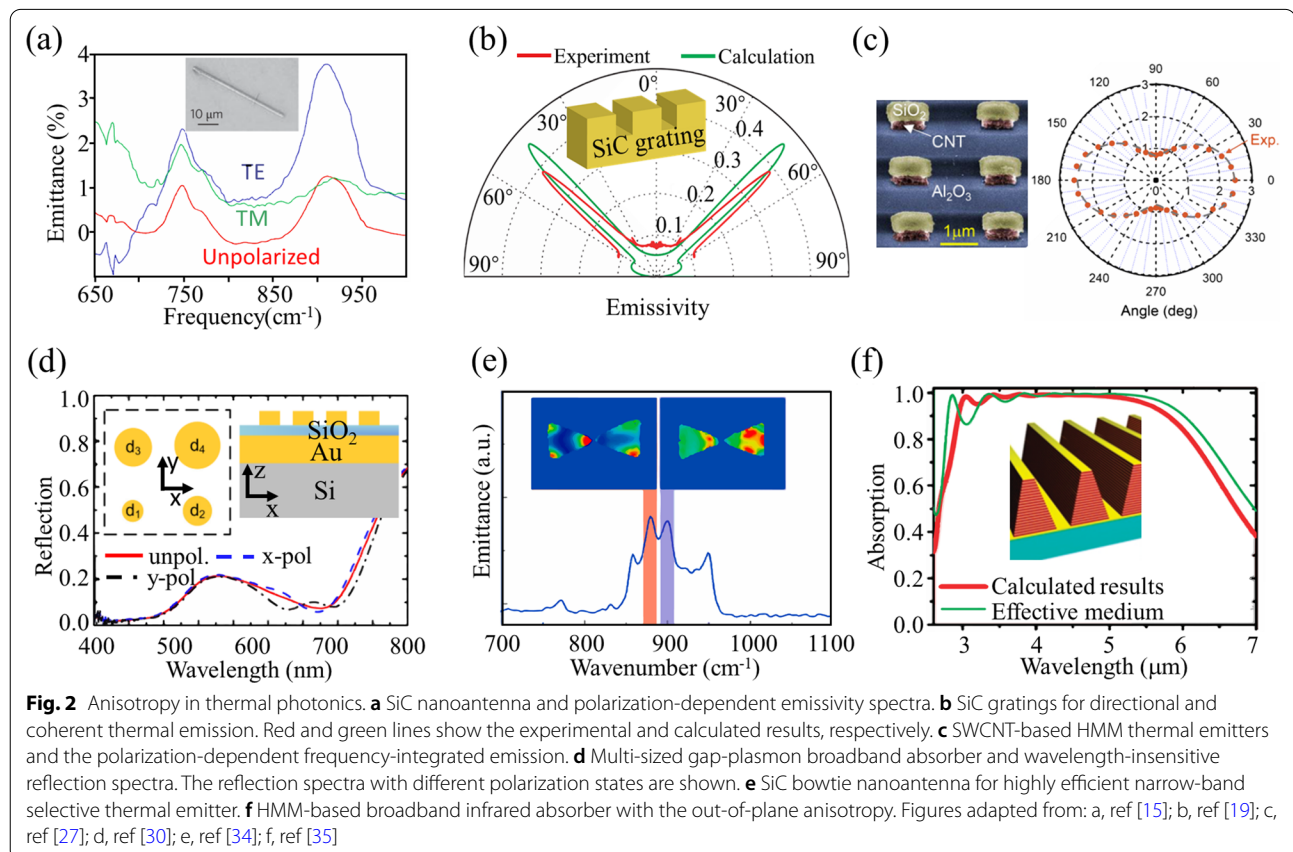
## 2 Breaking geometric symmetries

In this section, we review the physical consequences of breaking geometric symmetries on the absorptivity and emissivity of thermal emitters. We discuss the breaking of geometric symmetries by introducing anisotropy, aperiodicity, and chirality.

### 2.1 Anisotropy

A conventional thermal emitter emits omnidirectional, broadband, incoherent and unpolarized thermal radiation in space. With the introduction of anisotropy to metamaterials-based thermal emitters, one can expect distinct thermal emission properties in different directions. Amongst a plethora of metamaterials, isotropy can be broken along in-plane or out-of-plane directions, enabling selective control of emission properties like polarization, bandwidth, and coherence.

Figure 2a shows a silicon carbide nanorod optical antenna-based thermal emitter. The structure is a one-dimensional (1D) nanorod with a strong in-plane anisotropy [15]. It possesses an approximate translational



invariance along the nanorod axis and a mirror symmetry perpendicular to the nanorod axis. As a result, the structure supports TE and TM polarized modes that are orthogonal and well-separated in frequency. The combination of size-dependent Mie resonant modes and material-dependent optical phonon responses leads to highly efficient and wavelength-selective polarized thermal emission in the mid-infrared frequency range. Such optical antenna-based directional thermal emitters may find applications for communications [16]. Besides polarization control, such nanorod structures are also used to realize tunable narrowband thermal emitters [17, 18].

Grating is another widely used structure that breaks in-plane isotropy. As shown in Fig. 2b, Greffet et al. proposed a SiC grating to engineer the directionality, bandwidth, and coherence of thermal emission [19]. Such coherent thermal emission originates from the delocalized excitation of surface-phonon polaritons (SPhP). The periodicity of the grating compensates for the wavevector mismatch so that the SPhP modes can couple to free space. The in-plane anisotropy of the grating leads to polarization-dependent thermal emission [20, 21]. Ito et al. proposed a narrowband thermal emitter that consists of a Si grating suspended on a SiC plate. Its air-gap size-dependent emissivity clearly shows Fabry-Pérot fringes in spectra [22]. To extend the functionality of SiC-based gratings, Chalabi et al. proposed thermal lenses for focusing the thermal emission to a focal line in space [23]. The carefully designed nonperiodic structures create a space-dependent phase distribution for the scattered waves, resulting in constructive interference between all scattered waves at the focal line. The thermal lens may be suitable for photothermal applications based on selective heating nanostructures [24].

Beyond conventional anisotropic materials, hyperbolic metamaterials (HMM) possess extremely anisotropic permittivity tensors, exhibiting many useful properties like negative refraction and enhancement of spontaneous emission [25, 26]. For thermal radiation control, Gao et al. proposed an aligned single-walled carbon nanotube (SWCNT) film-based HMM [27], the strong in-plane anisotropy enables the polarization-dependent thermal emission, see Fig. 2c. The permittivity tensor has different signs in its diagonal components describing the direction parallel ( $\epsilon_{\parallel}$ ) and perpendicular ( $\epsilon_{\perp}$ ) to the SWCNT axis in mid-infrared wavelengths; metal-like  $\epsilon_{\parallel}$  and dielectric-like  $\epsilon_{\perp}$  result in enhanced and suppressed emissivity for different polarizations, respectively. Moreover, the film thickness can be readily tuned by simply stacking multiple layers; this allows for the simple and cost-effective fabrication of devices relying on macroscopically 1D properties of aligned carbon nanotube assemblies [28]. Besides, the extremely small diameters, the excellent

thermal conductivity, and the tolerance to high temperatures enable SWCNT well-suited for applications in thermal photonics [29].

Another approach to breaking the in-plane isotropy is to combine multiple resonators or meta-atoms in a single unit cell. The inter-particle coupling between periodic meta-atoms array may lead to angular or polarization-dependent but broadband or multiband responses. As shown in Fig. 2d, Nielsen et al. experimentally demonstrated a broadband efficient absorber based on gap plasmon [30]. For a single resonator, the gap plasmon resonant wavelength is easily controlled by modifying the diameter of meta-atoms and the gap size. For multisized resonators, the absorption efficiency and resonant wavelength are sensitive to the near-field coupling inside a supercell. The broadband absorption is required in thin-film based photovoltaic applications [31]. With careful geometric optimization of meta-atoms, broadband and near-perfect absorbers or thermal emitters are feasible for irregular meta-arrays [13, 32, 33]. Disordered or aperiodic metamaterials with reduced symmetry will be reviewed in Section "Aperiodicity and randomness".

Enhancing the local electromagnetic fields is an effective way to manipulate the properties of thermal emission. In Fig. 2e, Wang et al. reported a SiC bow-tie nanoantenna to tune bandwidth, coherence, and frequency of thermal emission, which is based on the near-field SPhP coupling at the gap [34]. SPhP modes are strongly enhanced at the tips of two adjacent triangles; such a "hot spot" effect is sensitive to the gap size. Moreover, for two modes in the middle of the spectrum, dipole-like surface charge distribution is mainly concentrated at the tips of triangles, and hence the corresponding emission peaks depend strongly on the gap size.

For out-of-plane anisotropic structures, as shown in Fig. 2f, Cui et al. proposed a sawtooth anisotropic metamaterial slab to expand the infrared absorption band [35]. A periodical sawtooth array is composed of metal/dielectric pair with a sub-wavelength size and a gradually changed width. The structure is designed to achieve non-resonant slow light trapping by engineering the dispersion of surface modes with TM polarization [36, 37]. Consequently, the absorption is near unity over a broad frequency range.

## 2.2 Aperiodicity and randomness

Periodic configuration is probably the most widely used configuration in meta-array-based thermal photonics. Thanks to translational symmetry, the Bloch theorem could greatly simplify the analysis of the system. However, many engineered structures don't possess strict translational symmetry, which gives extra freedom in the design of metamaterials [38, 39]. Aperiodic multilayer



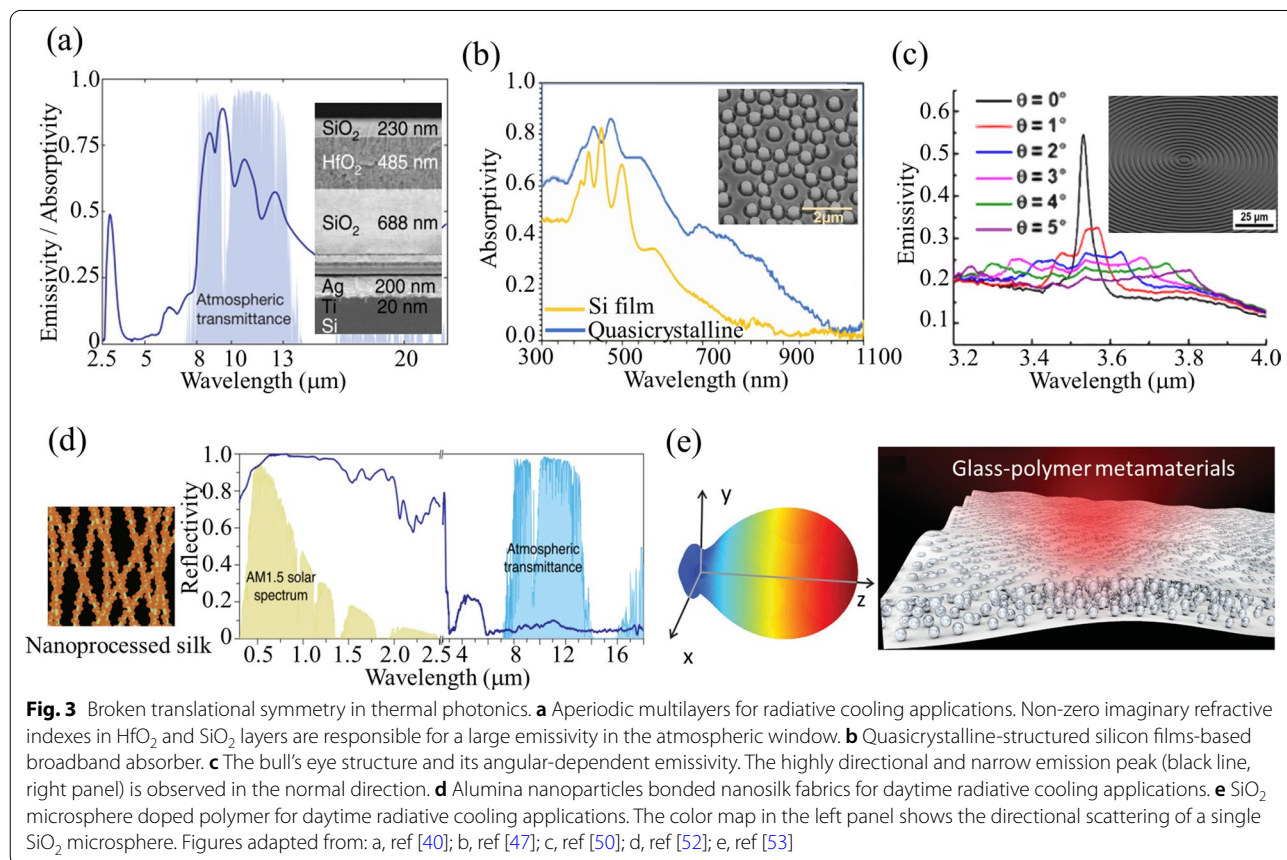
optical coatings are one of the simplest cases in this category.

As shown in Fig. 3a, Raman et al. proposed and experimentally demonstrated an optical thin-film with aperiodic multilayers for day-time radiative cooling applications [40]. The thin film consists of seven SiO<sub>2</sub> and HfO<sub>2</sub> alternative layers with different thicknesses, enabling broadband control of thermal radiation. The structure achieves broadband solar reflection and selective thermal emission in mid-infrared frequencies. The four thin layers at the bottom enhance the reflectivity in the solar spectrum while the three thick layers at the top enhance the emissivity in the mid-infrared wavelength range where the atmosphere is transparent. Aperiodic multilayer thin films can also be designed for selective and narrow-band thermal emitters [41–43].

Quasicrystalline structures are quasi-periodic. They have long-range order but lack translational symmetry [44–46]. Periodic structures strongly and coherently enhance optical interference and absorption. In contrast, quasicrystals possess some degree of disorders, enabling random light trapping and broadband optical absorption or thermal radiation [38, 39]. As shown in Fig. 3b, Xavier et al. reported a quasicrystalline-structured silicon

films-based broadband absorber [47]. The structure has a ten-fold transversely quasicrystalline lattice. Like the periodic structures, a quasi-periodic structure exhibits a well-defined discrete far-field diffraction pattern. Unlike periodic structures, however, the quasiperiodic structure exhibits a dense Fourier spectrum and a weaker angular dependence in its optical absorption and thermal radiation properties [48]. To further enhance the averaged absorptivity for broadband optical absorption, Mercier et al. demonstrated infinite-symmetry 2D Fibonacci patterning to improve the power conversion efficiency of Si solar cells, whose performance outperforms photonic quasicrystalline structures with 12-fold symmetry and photonic crystals with a triangular lattice [49].

In Fig. 3c, the Bull’s eye grating is a standalone structure for obtaining highly directional and efficient light emission and thermal radiation. Park et al. experimentally demonstrated a bull’s eye structure composed of tungsten and molybdenum concentric grooves for realizing a narrow band and directional thermal beam [50]. The structure hosts thermally excited surface-plasmon polaritons that can enhance optical absorption and thermal emission at resonant wavelengths. The circular symmetry enables highly directional thermal emission in the



normal direction. The highly directional thermal beam can be applied as nanostructured incandescent light sources [51].

Many chemically synthesized nanocomposites lack translational symmetry and long-range order. However, the cost-effective and scalable manufacturing process for such nanocomposites is well-suited for large-area energy applications. As shown in Fig. 3d, Zhu et al. synthesized nanoprocessed silk for daytime radiative cooling [52]. Silk is a good natural material for radiative cooling: Its nanofiber-like geometry enhances the overall reflectivity in the solar spectrum, and the vibrational modes of amino acids increase the emissivity in the atmospheric window. However, natural silk exhibits undesirable absorption at ultraviolet wavelengths that preclude net daytime cooling. To reduce ultraviolet absorption, Zhu et al. bonded alumina nanoparticles to silk-based fabrics. Such hierarchical microstructures have the right sizes and large refractive index contrast to strongly scatter the ultraviolet light. Using randomly distributed nanoparticles is another practical way for scalable daytime radiative cooling applications. In Fig. 3e, Zhai et al. utilized glass-polymer hybrid metamaterials to selectively control optical reflection in the solar spectrum and thermal radiation in mid-infrared wavelengths [53]. SiO<sub>2</sub> microspheres introduce a strong forward Mie scattering near the phonon polariton resonance. Moreover, ensembles of randomly dispersed microspheres can be regarded as an effective medium and the radiation wavelength-comparable microspheres broaden the emissive band in the atmospheric window.

### 2.3 Chirality

In general, an optical structure with broken mirror symmetry and inversion symmetry can generate chiral effects and exhibit different responses between left-handed and right-handed circularly polarized lights [54, 55]. The chiral response of a structure is characterized by the optical chirality density ( $C$ ), defined as [56–59],

$$C = \frac{\varepsilon_0}{2} \mathbf{E}^* \cdot \nabla \times \mathbf{E} + \frac{1}{2\mu_0} \mathbf{B}^* \cdot \nabla \times \mathbf{B}, \quad (1)$$

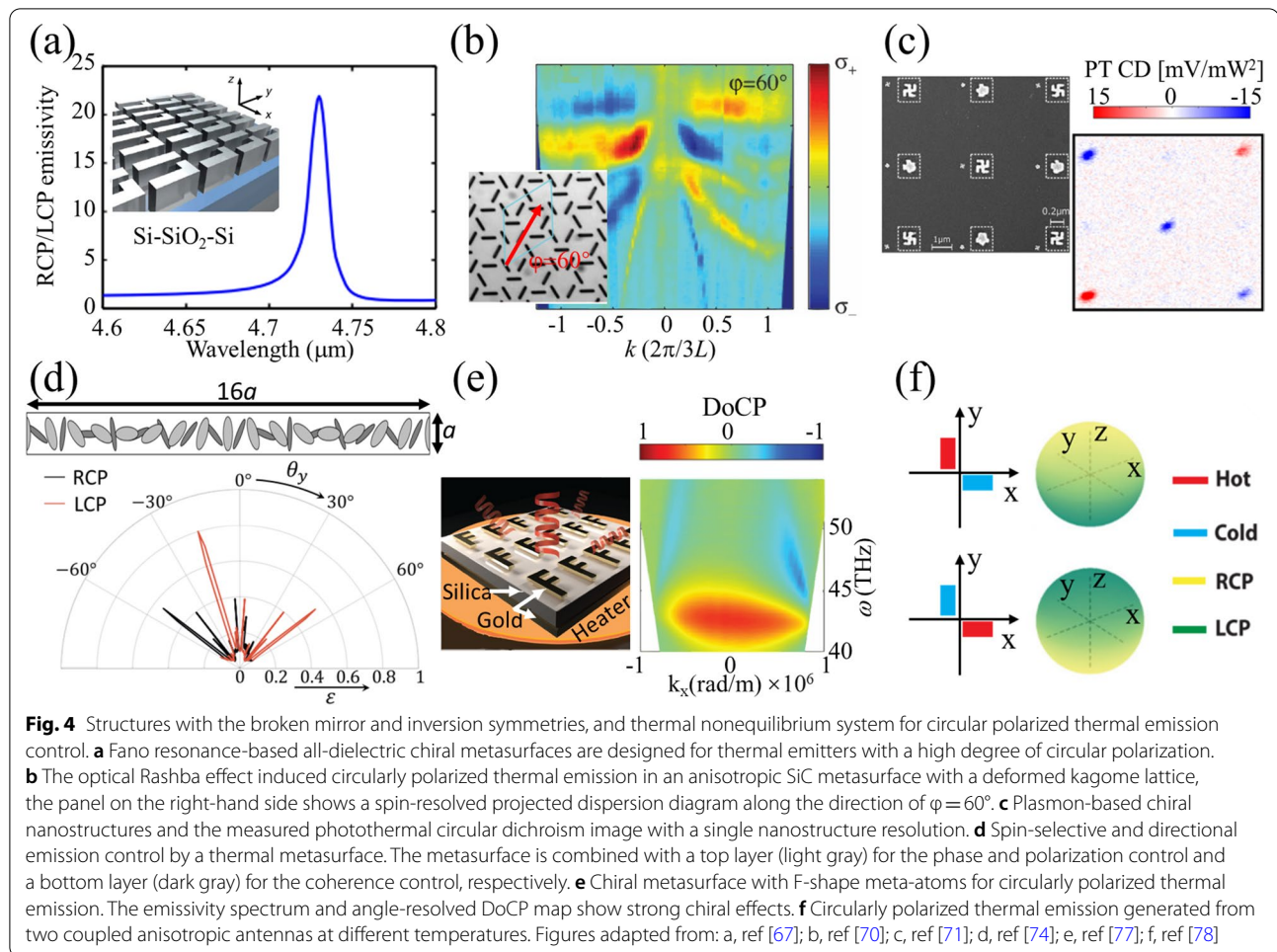
Here,  $\mathbf{E}$  and  $\mathbf{B}$  are complex electric and magnetic fields, the asterisk sign denotes the complex conjugate,  $\varepsilon_0$  and  $\mu_0$  are permittivity and permeability in vacuum, respectively. Therefore, to enhance the chiral response of a structure, Eq. (1) implies that one needs to enhance the out-of-phase local electric and magnetic fields near the structure.  $C$  is related to other quantities that characterize differential optical responses for left-handed and right-handed circularly polarized (LCP and RCP) lights, such as circular dichroism (CD) and asymmetry  $g$ -factor [56, 57]. In thermal photonics, chiral geometries bring

new opportunities and functionalities to circularly polarized thermal emission and photothermal applications [60–64]. Here, we emphasize that breaking mirror and inversion symmetry is a necessary but not sufficient condition for realizing chiral thermal emission. The structures need to be carefully designed to exhibit strong chirality dependence in thermal emission [65, 66].

As shown in Fig. 4a, an all-dielectric chiral metasurface is designed and fabricated for narrow band absorption and numerically evaluated for circularly polarized thermal emission [67]. Fano resonance is obtained from the chiral geometry of meta-molecules via the coupling between the bright dipole modes and the dark quadrupole modes. The chiral geometry simultaneously breaks the in-plane mirror and inversion symmetry, which is the key to generating differential optical responses to LCP and RCP lights. An infrared-absorbing slab is introduced beneath the chiral metasurface. The Fano resonance in the combined structure has a large quality factor, which is beneficial for a narrow-band thermal emitter with a high degree of circular polarization (DoCP).

The optical Rashba effect is a phenomenon of spin-orbital interaction of light that can occur when inversion symmetry is broken. This effect manifests as a spin-dependent split of the dispersion relation of photons and can be used to generate circularly polarized emission [68, 69]. In Fig. 4b, the SiC metasurface with a deformed kagome lattice enables thermal emissions with high DoCP observed in the angle-resolved thermal emission spectrum, due to the spin-dependent split of the dispersion relation of the radiative modes [70]. The broken inversion symmetry removes the spin degeneracy and reciprocity guarantees that two modes with opposite wavenumbers have the same frequency [69]. The strength of spin splitting is proportional to the gradient of the space-variant orientation angle of meta-atoms.

To visualize optical chirality at a single nanoparticle level, as shown in Fig. 4c, Spaeth et al. studied chiral plasmonic nanostructures with the combination of circular dichroism and photothermal imaging [71]. It is well-known that plasmon-based chiral nanostructures can enhance chiral signals like circular dichroism and asymmetry  $g$ -factor [54, 72]. A single chiral nanostructure, however, usually produces only very weak chiral signals that are undetectable by conventional circular dichroism spectroscopy. When light is incident on a nanoparticle, the absorbed energy heats the surrounding medium and creates a thermal lens. A heating beam (pump) with periodically modulated circular polarization states is utilized in Ref. [71], the differential absorption between two circularly polarized lights results in the time-dependent variation of the thermal lens surrounding the nanostructure. When another tightly focused beam is introduced



as a probe beam, the strength of the thermal lens effect can be detected by the optical interference phenomenon between the reflected light and the thermal lens-induced backscattered light. This novel photothermal imaging technique can generate a circular dichroism image with sufficient resolution to detect a single chiral nanoparticle [73].

Chiral nanostructures are not only limited to in-plane geometry with broken symmetries, Overvig et al. reported a double-layered thermal metasurface for circularly polarized thermal emission control [74]. As shown in Fig. 4d, the phase-gradient metasurface consists of two layers of Si nanopillar meta-atoms: light gray colored Si nanopillars at the top layer and dark gray colored nanopillars at the bottom layer. The chirality is introduced and varied by different orientation angles of interlayer meta-atoms, exhibiting the broken mirror and space-inversion symmetries. The top layer controls the local phase and polarization of thermal emission, and the bottom layer controls the temporal and spatial coherence of partially polarized thermal emission. The enhanced main lobe of

LCP emission is observed around a  $-20^\circ$  orientation angle relative to the  $y$ -axis ( $\theta_y = -20^\circ$ ), resulting from the geometric phase engineering in the design of both layers. In contrast, other side lobes of emission exhibit an angular emission behavior that is similar between opposite spins of thermal photons. Additionally, the highly directional thermal emission implies improved spatial coherence, which originates from the symmetry-protected bound states in the continuum supported at the bottom layer [75, 76].

To systematically elucidate the impact of different broken symmetries on circularly polarized thermal emission control, Wang et al. fabricated gold–silica–gold metasurfaces with F-shaped meta-units [77]. In Fig. 4e, a left-handed circularly polarized thermal emission peak ( $\sigma^+$ ) appears at  $7\ \mu\text{m}$ , in contrast, the right-handed circularly polarized thermal emission ( $\sigma^-$ ) is weak and flat in wavelength. The difference between the two circular polarizations originates from the distribution of optical density of chirality in F-shaped nanostructures. In general, mirror symmetry must be broken to obtain thermal emission



with a large DoCP. Moreover, as shown in the measured angle-resolved thermal emission spectra in Fig. 4e, an asymmetric DoCP pattern is observed in the  $k$ -space for a structure that simultaneously breaks inversion and mirror symmetries. On the contrary, a symmetric DoCP pattern is observed in the  $k$ -space for a structure that preserves inversion or fourfold rotation symmetry. Besides circularly polarized thermal emitters, plasmon-based chiral metasurfaces also have many applications in chirality-based photothermal effect [64].

Beyond chirality induced by breaking geometrical symmetries, Khandekar et al. investigated circularly polarized thermal emissions from coupled antennas in nonequilibrium [78]. As shown in Fig. 4f, two anisotropic antennas (two bars with red and blue colors) are perpendicularly arranged with a subwavelength-sized separation. These two antennas are kept at different temperatures. From the analysis of fluctuational electrodynamics, the circular polarization or the handedness of thermal emission to the direction perpendicular to the two antennas is switchable by reversing the temperature of two antennas, but the total spin angular momentum of thermal emission, summed over all directions, is still zero. Furthermore, DoCP and the directionality of circularly polarized thermal emission depend on the emission wavelength, temperature difference, polarizabilities, and geometric parameters of antennas. This novel mechanism may lead to practical applications like reconfigurable circularly-polarized light-emitting diodes [79].

### 3 Engineering mode symmetries

Above we have focused on the symmetry breaking of the photonic structures. In this section, we discuss the symmetry breaking of the photonic modes and its consequences on thermal radiation.

#### 3.1 Fano resonance

In photonics, Fano resonance occurs when a resonant mode is coupled to a slowly varying background [80–84]. Fano resonances manifest sharp variations in the transmission, reflection, and absorption spectra, which can be used in photonic and thermal photonic applications [85–88]. The asymmetric line shape is due to the destructive interference between the resonant mode and the continuous background. It can be phenomenologically described by the Fano formula. [82]

$$\sigma = \frac{(\Omega + q)^2}{\Omega^2 + 1} \quad (2)$$

here  $\sigma$  describes the line-shape of scattering cross-section of nanostructures near the resonance,  $\Omega = 2(E - E_0)/\Gamma$ ,  $E_0$  and  $\Gamma$  denote resonant energy and width.  $q$  is the asymmetric parameter that controls the line-shape. The

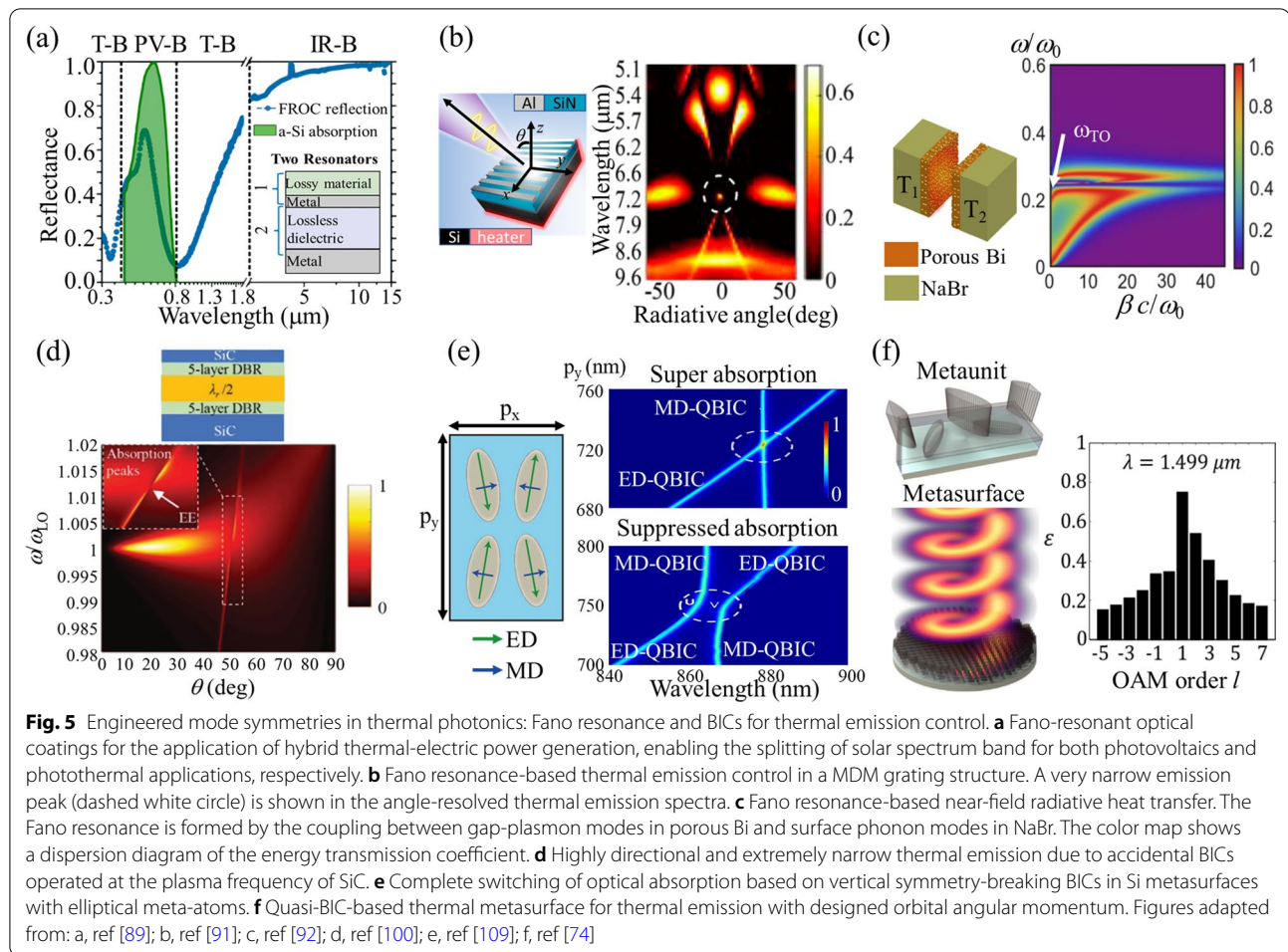
quality factor is defined as  $Q = 2E_0/\Gamma$  which is a dimensionless parameter that characterizes the damping of a resonator. Although creating Fano resonances does not require breaking geometric symmetries, the detailed physics of Fano interference is affected when the symmetry of the structure is broken, which affects the symmetry properties of the modes and the coupling between distinct nanophotonic structures.

Based on two coupled resonant cavities with distinct  $Q$ -factors, Elkabbash et al. proposed and experimentally demonstrated Fano-resonant optical coatings (FROC) for the hybrid thermal-electric power (HTEP) generation, which splits the solar spectrum band for both photovoltaics and photothermal applications [89]. The structure of such optical coating much simplifies the design and fabrication processes compared with other nanophotonic structures. In Fig. 5a, resonator 1 is a lossy cavity, resulting in a broad absorption band in the solar spectrum. In contrast, resonator 2 is a metal-dielectric-metal cavity with a lossless dielectric, resulting in a narrow absorption band near the specific wavelength. The destructive interference between two resonators generates an asymmetric reflection peak spectrally overlapping with the absorption band of amorphous Si and the reflected photons could be used in photovoltaic cells. Besides, FROC exhibits strong absorption in the remainder of the solar spectrum and suppressed absorption outside the solar spectrum, enabling the improvement of optothermal efficiency of solar absorbers [90].

Grating structures can also host Fano resonances. Exploiting the parity symmetry of eigenmodes, Zhang et al. analyzed and observed a Fano resonance-based narrow band thermal emission in an Al/SiN/Al grating structure [91]. As shown in Fig. 5b, the grating possesses two types of eigenmodes, i.e., meta-atom size-dependent metal-dielectric-metal (MDM) cavity modes, and periodicity-dependent surface lattice modes. At normal incidence, the even order MDM cavity modes are dark modes with even parity, and surface lattice modes are bright modes with odd parity. Adjusting the meta-atom size and the periodicity, Fano resonances can be formed by the spectral and spatial overlap of dark and bright modes, leading to a very narrow thermal emission peak in the normal direction, as shown in the right panel of Fig. 5b (dashed white circle).

Fano resonances also play an important role in near-field radiative heat transfer (NFRHT). Pérez-Rodríguez et al. proposed a metamaterial for selectively tailoring NFRHT based on polaritonic and plasmonic modes hybridization [92]. As shown in Fig. 5c, the symmetric nanocavity consists of polaritonic material NaBr and porous Bismuth on both sides with a large temperature difference. The evanescent gap-plasmon and SPhPs





modes can greatly enhance the efficiency of radiative heat transfer through the nano-sized gap. A Fano resonance is observed near the spectral overlapped region of two evanescent modes, due to the mode splitting induced by the strong coupling between gap-plasmon modes (bright modes) and transverse SPhPs modes (dark modes). The asymmetric line shape shows an opening of the thermal bandgap and the enhancement of energy transmission coefficient near the frequency of transverse phonon mode ( $\omega_{TO}$ ), indicating the suppressed and enhanced NFRHT inside the nanocavity respectively.

### 3.2 Bound states in the continuum (BIC)

Bound states in the continuum are localized states inside the continuum of radiated waves, which can be regarded as a Fano resonance with an infinite Q-factor [93, 94]. In general, symmetry-protected BICs and accidental BICs can respectively appear at  $\Gamma$ -point and off- $\Gamma$  point with an infinite Q-factor [80, 95–99]. Sakotic et al. numerically demonstrated Berreman modes-based BICs at epsilon-near-zero (ENZ) wavelengths in SiC slab structures,

which can be used as an ultranarrow band thermal emitter [100]. In physics, a bound state possesses no radiating far-fields. For a single particle BICs, electric and magnetic fields must be zero anywhere with a finite permittivity or permeability, due to the continuity of the fields. Thus, single particle BICs cannot exist in a compact structure [94, 101]. In contrast, single particle BIC can exist when a material with zero permittivity or permeability is introduced. In particular, ENZ materials-based structures can support single-particle quasi-BICs [101, 102]. For a single SiC slab, at normal incidence, symmetry-protected BICs are obtained at the ENZ frequency, i.e., longitudinal phonon frequency of SiC( $\omega_{LO}$ ), which can be regarded as a Fano resonance with near-zero linewidth [103]. The non-zero material loss induces the conversion from BICs to quasi-BICs [104]. As shown in Fig. 5d, at oblique incidence in multilayer slabs, accidental BICs are formed by the destructive interference between the central dielectric gap-size dependent Fabry-Pérot (FP) modes and volume plasmon modes at the plasma frequency [105]. The use of distributed Bragg reflectors (DBR) further narrows

the thermal emission peaks. To reduce the transmittance and enhance the emissivity, two asymmetric SiC layers are introduced at the top and bottom layers. The result shows a highly directional and extremely narrowband thermal emission near the ENZ wavelength.

Symmetry-protected BICs can also emerge in dielectric metasurfaces [106–108]. As shown in Fig. 5e, Tian et al. proposed a strategy to switch optical absorption between enhanced and suppressed states by controlling the vertical symmetry of the refractive index surrounding a high-Q crystalline Si metasurface [109]. The metasurface consists of elliptical meta-atoms that support Mie-resonance-based electric dipole (ED) and magnetic dipole (MD) modes, respectively. When the in-plane inversion symmetry is preserved, two BIC modes, ED-BIC and MD-BIC, can be formed at  $\Gamma$ -point due to the mismatched symmetry between BIC modes and the zero-order diffraction [80, 97, 107]. Then, distorting elliptical meta-atoms, two BIC modes convert to two quasi-BIC modes with a finite but large Q-factor due to the broken in-plane inversion symmetry [107]. Two quasi-BIC modes are orthogonal when the superstrate and substrate have the same refractive indexes. With a non-zero material loss, the absorption of the Si metasurface is strongly enhanced at two wavelengths of ED- and MD-BICs. When the superstrate and substrate have different refractive indexes, the two quasi-BIC modes can couple to each other creating a modal gap within which the absorption is suppressed. Controlling the vertical symmetry surrounding the metasurface, one therefore achieves a complete switching of optical absorption. Such an idea has been experimentally confirmed in Ref. [110].

Based on the nonlocal property of symmetry-protected quasi-BIC states, Overvig et al. proposed a principle and design rules for comprehensive control of thermal emission by a hybrid metasurface [74]. For conventional optical metasurfaces, like independent scatters, a meta-unit enables local manipulation of the wavefront, phase, and amplitude of the coherent light. For a thermal metasurface, such local metasurfaces are not sufficient to control the partially coherent thermal emission. Instead, a thermal metasurface requires simultaneously local and nonlocal responses. As shown in Fig. 5f, an example of thermal metasurfaces is composed of a top layer of tilted dielectric meta-monomers with local responses and a bottom layer of dielectric asymmetric meta-dimers with nonlocal responses. The nonlocal layer controls the coherence, while the local layer controls the phase. One functionality of such hybrid metasurfaces is to generate orbital angular momentum (OAM) of thermal light. Figure 5f shows the numerical demonstration of preferential thermal emission with the first-order OAM. The hybrid local-nonlocal thermal metasurfaces are promising for

comprehensive thermal emission control including directionality, coherence, focusing, and angular momenta [74, 76].

## 4 Breaking reciprocity

Reciprocity is a fundamental internal symmetry of Maxwell's equations [9]. It imposes direct constraints on basic optical phenomena including transmission [111], reflection [112], absorption, and emission [10, 113]. In thermal radiation, reciprocity implies Kirchhoff's law that relates the angular spectral absorptivity and emissivity of a reciprocal emitter. Conversely, the capability of breaking reciprocity enables significant new opportunities for nonreciprocal thermal emission.

### 4.1 Magneto-optical effect

In the process of thermal radiation, Kirchhoff's law of thermal radiation governs the detailed balance between the angular spectral absorptivity ( $\alpha$ ) and emissivity ( $e$ ) of a thermal emitter.

$$\alpha(\omega, -\hat{n}, \hat{p}) = e(\omega, \hat{n}, \hat{p}^*) \quad (3)$$

here  $\omega$  is the angular frequency,  $\hat{n}$  is the direction, and  $\hat{p}$  and  $\hat{p}^*$  are the polarization vector and the corresponding complex conjugate. Kirchhoff's law is a consequence of Lorentz reciprocity. Hence, Kirchhoff's law can be violated in a nonreciprocal system. When Lorentz reciprocity is broken, the absorptivity and emissivity may not be equal at the specific frequency and direction [114]. Note the nonreciprocal radiative exchange process doesn't violate the second law of thermodynamics. Exploiting the nonreciprocity could greatly improve the conversion efficiency in solar energy harvesting applications compared with its reciprocal counterpart [115–117]. It is known that for solar energy harvesting, reaching the Landsberg limit, which represents the ultimate efficiency limit, requires reciprocity breaking [118].

To break reciprocity, one can use magneto-optical materials or a dynamic time modulation. With an external magnetic field, magneto-optical (MO) materials possess an asymmetric permittivity tensor, enabling the breaking of Lorentz reciprocity in a linear and passive system. Magnetized MO materials are widely used in communication systems for optical isolation [119, 120]. In thermal photonics, Zhu et al. pointed out that detailed balance can be violated in nonreciprocal systems [114]. They also numerically proposed a highly doped InAs-based grating structure operating in the reflection configuration for near-complete violate the detailed balance between  $\alpha$  and  $e$ . Under a static external magnetic field, InAs is a MO material at infrared frequencies with large asymmetric off-diagonal permittivity components. With

the use of the grating structure, the strong nonreciprocity induces a large frequency deviation between  $\alpha$  and  $e$  as shown in Fig. 6a. Note the integration of absorptivity and emissivity over all angles and polarizations must be equal, as required by the second law of thermodynamics [121]. In other words, the detailed balance between  $\alpha(\omega, -\hat{n}, \hat{p}^*)$  and  $e(\omega, \hat{n}, \hat{p}^*)$  can be violated for a nonreciprocal thermal emitter, but the integrated  $\alpha$  and  $e$  must be balanced for both reciprocal and nonreciprocal systems. Different from the reflection-based nonreciprocal thermal emitters

discussed above, Park et al. proposed a semitransparent structure enabling the violation of Kirchhoff's law in the transmission configuration, leading to near-unity absorptivity at the incident side and near-unity emissivity at the transmission side [122].

As shown in Fig. 6b, Shayegan et al. reported an experimental demonstration of amorphous Si grating structure loaded InAs nonreciprocal absorber or thermal emitter [123]. This work is related to earlier theoretical works by Zhao et al. [124], which showed that a similar

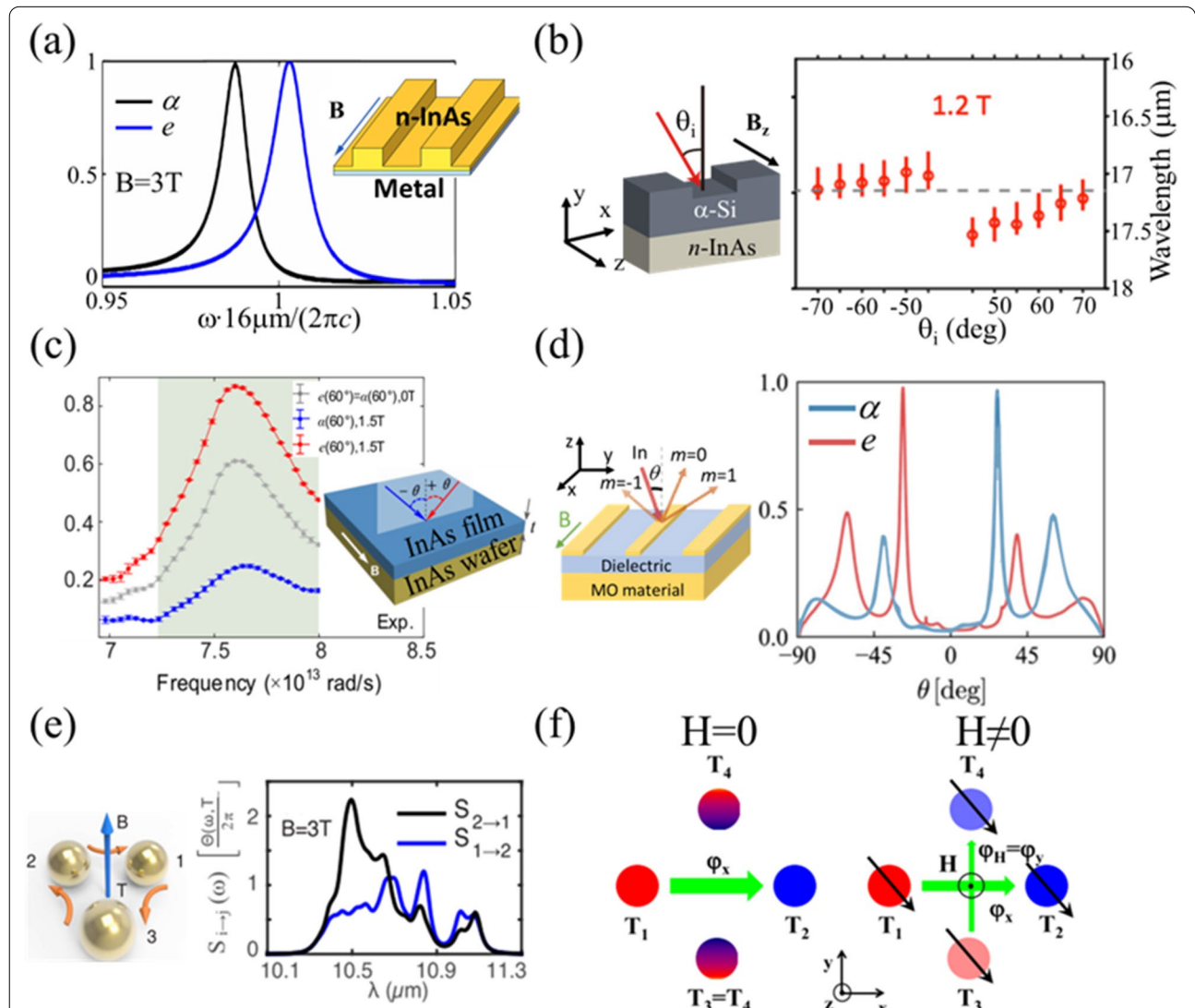


**Fig. 6** Broken reciprocity in thermal photonics by using magneto-optical effect. **a** MO grating enables the near-complete violation of detailed balance between  $\alpha$  and  $e$ . **b** Incident angle-resolved nonreciprocal absorption phenomenon measured from Si grating loaded highly-doped InAs structures. Circles and error bars denote the maximum absorption and the 5% variation wavelength range from maximum absorption, respectively. **c** Berreman mode induced a large violation of Kirchhoff's law in ultrathin InAs films at ENZ wavelengths. **d** A MO material-based nonreciprocal grating with a compound symmetry that illustrates the adjoint Kirchhoff's law. **e** Persistent heat current generated in a nonreciprocal many-body system at thermal equilibrium. **f** Photon thermal Hall effect in a nonreciprocal many-body system. The transverse temperature difference is formed when the many-body system is magnetized. Figures adapted from: a, ref [114]; b, ref [123]; c, ref [128]; d, ref [10]; e, ref [135]; f, ref [141]



configuration can achieve a strong violation of detailed balance with a magnetic field that is far smaller as compared with the original design of Zhu et al. [114]. Under an external magnetic field, the magneto-optical property of heavily doped *n*-InAs can be described by the Drude model with nonzero off-diagonal permittivity values. The Si grating is designed to support the guided-mode resonance (GMR) near the ENZ wavelength of doped InAs. The ENZ wavelength of magneto-optical materials is attractive for the demonstration of non-reciprocal effects due to the large ratio between off-diagonal and diagonal permittivities [125]. The GMR structure is preferentially coupled to p-polarized propagated modes (electric fields in the *x*-*y* plane) whose absorption peaks strongly shift under the applied magnetic field in Voigt configuration (i.e., the externally applied B field is along the *z*-direction). The detection of the shift of the resonant peak due to the external magnetic field in an angle-resolved measurement provides the signature of the nonreciprocal absorption. The asymmetric behavior of the resonant peaks with respect to the angles of incidence is observed in the absorption spectrum at  $B_z = 1.2$  T. The asymmetry originates from the asymmetry in dispersion relation of GMR as induced by the magnetic field [126, 127].

Using the same magneto-optical material, as shown in Fig. 6c, Liu et al. experimentally observed a strong violation of Kirchhoff's law and systematically engineered the wavelength of nonreciprocal thermal emission in nanostructures with ultrathin highly-doped InAs films at ENZ wavelengths [128]. The maximum violated strength of  $|\alpha - \varepsilon|$  is larger than 0.6 at  $B_z = 1.5$  T, resulting from asymmetric radiative Berreman modes (above the light-line) supported in the ultrathin InAs films. Berreman modes are strongly dependent on doping concentration and thickness of InAs thin films, enabling InAs multilayers with gradually changed doping concentration for broadband nonreciprocal thermal emitters. Additionally, as the other type of nonreciprocal modes in the structure, surface ENZ modes below the light-line in the ultrathin InAs films can also be excited under a grating-assisted excitation, leading to multiband nonreciprocal thermal emitters. Besides MO materials, the magnetic Weyl semimetal is another promising candidate for nonreciprocal thermal emitters without the applied magnetic field. Its large off-diagonal permittivity originates from the large anomalous Hall effect [129–133]. Broadband circularly polarized thermal light is also numerically demonstrated in magnetic Weyl semimetals [134].

These recent developments of nonreciprocal thermal emitters, therefore, require a deeper understanding and proper generalization of conventional Kirchhoff's law. Guo, Zhao, and Fan developed such a fundamental framework based on group theory [10]. Their work

elucidates the general relation between the angular spectral absorptivity  $\alpha(\omega, -\hat{n}, \hat{p})$  and emissivity  $e(\omega, \hat{n}', \hat{p}')$  for any thermal emitter including nonreciprocal ones. Here  $-\hat{n}$  and  $\hat{p}$  ( $\hat{n}'$  and  $\hat{p}'$ ) denote the direction and polarization of incoming (outgoing) waves, respectively. Their main results are as follows: First, they established a natural generalization of the conventional Kirchhoff's law, termed adjoint Kirchhoff's law, which also applies to nonreciprocal objects. They pointed out that, given any object, there exists a unique object, called its adjoint, obtained by an adjoint transformation [9]. A reciprocal object's adjoint is itself. A nonreciprocal object's adjoint is a different object; these two objects form a pair that are mutually adjoint. Adjoint Kirchhoff's law states that: the angular spectral absorptivity of one object equals the angular spectral emissivity of its adjoint. Then, using this law, they derived all the relations between absorptivity and emissivity for an arbitrary single thermal emitter. They pointed out that such relations are determined by the intrinsic symmetries of the system, which are characterized by a Shubnikov point group. This allows for a complete classification of all thermal emitters based on symmetries. Each class possesses its own set of laws that relates the angular spectral absorptivity and emissivity. As such, this work provides the theoretical foundation for the design and application of all thermal emitters, especially nonreciprocal ones. As an example, Fig. 6(d) shows a magneto-optical grating with a compound symmetry  $T\sigma_v(xz)$ , where  $T$  denotes the adjoint transformation and  $\sigma_v(xz)$  denotes the mirror operation with respect to the *xz* plane. Such a nonreciprocal grating violates Kirchhoff's law, e.g.,  $\alpha(\omega, \theta, p) \neq e(\omega, \theta, p)$  for the p-polarized light in the *yz* plane with an incident angle  $\theta$ . However, it still satisfies adjoint Kirchhoff's law, which requires that  $\alpha(\omega, \theta, p) = e(\omega, -\theta, p)$ .

The introduction of nonreciprocity can also generate unconventional physical effects in the NFRHT, especially in many-body systems [5]. Zhu et al. found a directional persistent heat current circulating inside a nonreciprocal many-body system at thermal equilibrium [135]. As shown in Fig. 6e, the system consists of three MO nanospheres at the same temperature. Without magnetization, the net heat current between body 1 and body 2 is zero, i.e., the clockwise heat current ( $S_{2 \rightarrow 1}$ ) and the counter-clockwise heat current ( $S_{1 \rightarrow 2}$ ) are equal, due to the Lorentz reciprocity. With out-of-plane magnetization, the nonreciprocity induces a clockwise net heat current ( $S_{2 \rightarrow 1} > S_{1 \rightarrow 2}$ ). Note  $S_{2 \rightarrow 1} = S_{1 \rightarrow 3} = S_{3 \rightarrow 2}$ , due to the three-fold rotation symmetry in the system. The zero net heat flow abides by the requirement of the second law of thermodynamics. Such persistent heat currents also exist for systems consisting of more bodies [136]. The directional



persistent heat flow in the above MO many-body systems should not be confused with thermal circulators, which work away from thermal equilibrium [137].

The photon thermal Hall effect is another related NFRHT phenomenon initially found in nonreciprocal many-body systems. In Fig. 6f, Ben-Abdallah proposed a system consisting of four MO particles. The size of MO particles is much smaller than the thermal wavelength. A longitudinal temperature difference is applied between body 1 and body 2. Without magnetization, only the longitudinal heat current exists and two transverse bodies have the same temperature, due to the mirror symmetry with respect to the  $xz$ -plane. With out-of-plane magnetization, a temperature difference develops in the transverse direction between body 3 and body 4 since the mirror symmetry is broken. As an extension, Ott et al. investigated the anomalous photon thermal Hall effect in Weyl semimetals-based many-body systems [138]. In contrast with the persistent heat current, the photon thermal Hall effect is not a uniquely nonreciprocal effect; it can arise in some reciprocal systems with broken-mirror symmetry. However, for systems with  $C_4$  rotational symmetry, the photon thermal Hall effect is uniquely nonreciprocal, and there is a direct connection between the persistent heat current and the photon thermal Hall effect. In the near-equilibrium regime, the magnitude of the photon thermal Hall effect is proportional to the temperature derivative of the persistent heat current [139].

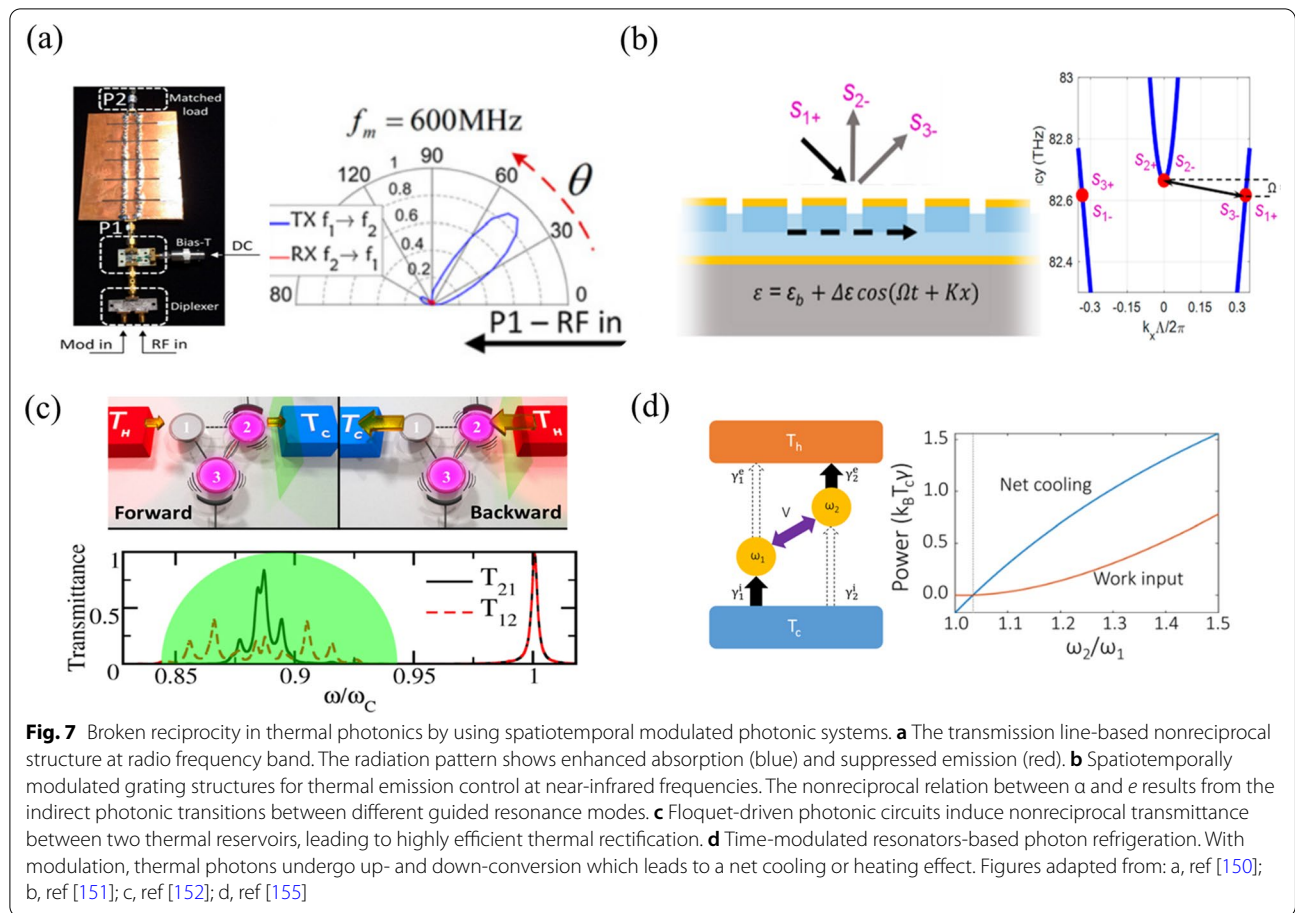
The concepts of adjoint symmetries and Shubnikov groups are also important in studying NFRHT. Guo and Fan systematically studied the constraints on reciprocal and non-reciprocal many-body radiative heat transfer imposed by symmetries and the second law of thermodynamics [140]. They showed that the symmetries of such a many-body system in general forms a Shubnikov group, and the constraints of the Shubnikov group on the heat transfer can be derived using a generalized reciprocity theorem. As an application, they provided a systematic approach to determining the existence of persistent heat current in arbitrary many-body systems.

#### 4.2 Spatiotemporal modulation

As a promising approach to breaking the Lorentz reciprocity without applied magnetic fields, the spatiotemporal modulation method attracts significant attention in nonreciprocal and topological photonics [142–146]. In general, spatiotemporal modulation can introduce linear momentum [142], angular momentum [147], or other physical quantities biasing with odd-symmetry under time-reversal operation to break reciprocity [145, 148, 149]. Two categories of spatiotemporally modulated structures for applications in thermal photonics are discussed in this review: waveguides and resonators.

For waveguides, based on traveling-wave modulation, Hadad et al. experimentally demonstrated a transmission line antenna for nonreciprocal emission control at radio frequency band [150]. As shown in Fig. 7a, under a spatiotemporal modulation of the voltage-dependent capacitors, an asymmetric intraband transition occurs between dispersion bands with different harmonic orders, resulting in the breaking of reciprocity between absorption ( $T_x$ , up-conversion) and emission ( $R_x$ , down-conversion). The asymmetric transition results from the phase-matching condition introduced by spatiotemporal modulation. At 600 MHz modulation frequency, the angle-resolved diagram shows strong nonreciprocal radiation patterns with enhanced absorption and suppressed emission. At near-infrared frequencies, Ghanekar et al. reported nonreciprocal thermal radiation in a dynamically modulated grating [151]. The modulated permittivity along the traveling wave direction introduces a shift in both wavevector and frequency in a guided resonance grating, leading to the broken time-reversal symmetry and the nonreciprocity. As a result, indirect photonic transitions between different guided resonance modes in the grating are dependent on the propagation direction. i.e., the phase-matching condition is fulfilled for the forward mode but not for the backward mode. As shown in Fig. 7b,  $S_{1+}$  corresponds to a forward incident wave,  $S_{2-}$  and  $S_{3-}$  correspond to two outgoing modes. A photonic transition occurs when the modulation matches the frequency and the wave vector for the transition  $S_{1+} \rightarrow S_{2-}$ . However, for the backward incident wave  $S_{3+}$ , the transition  $S_{3+} \rightarrow S_{2-}$  is forbidden due to the mismatched wave vector. Such an indirect photonic transition enables the violation of Kirchhoff's law when the loss is introduced in the grating. A complete nonreciprocal mode conversion can be realized when the modulation depth meets the critical coupling condition in the grating, resulting in an enhanced unequal emissivity and absorptivity at the resonance. Furthermore, a directional-dependent Rabi splitting phenomenon can also be observed in a strongly modulated system.

Based on time-modulated resonators, Fernández-Alcázar et al. proposed a Floquet-driven photonic circuit enabling highly efficient thermal rectification [152]. As shown in Fig. 7c, the thermal diode consists of three resonators: resonator 1 is unmodulated, resonator 2 and resonator 3 are periodically modulated with a Floquet-driven frequency. A temperature gradient is applied between two thermal reservoirs near two resonators, i.e.,  $T_{\text{left}} \neq T_{\text{right}}$ . The forward and the backward configurations are defined as  $T_{\text{left}} > T_{\text{right}}$  and  $T_{\text{left}} < T_{\text{right}}$ , respectively. Without modulation, temperature bias-induced thermal currents are reciprocal for both forward and backward configurations. With periodic modulation, the



degeneracy of the two counter-rotating modes in the photonic circuit is removed, resulting in nonreciprocal transmittance between two reservoirs. Such nonreciprocal phenomenon originates from the interference effects between states with different Floquet ladders (frequency harmonics) which is realized by angular momentum biasing in this 3-resonators system with rotational symmetry [153, 154]. Controlling the spectral emissivity of thermal reservoirs can enhance the nonreciprocal thermal emission, which may also be favorable for the design of thermal circulators.

As another key application in the use of temporal modulation for thermal emission control, Buddhiraju et al. proposed a time-modulated resonant system-based thermal photonic refrigerator, showing an active cooling mechanism via pumping residual heat from the cold side to the hot side [155]. As shown in Fig. 7d, a photonic refrigerator is composed of two distinct resonant modes with different resonant frequencies  $\omega_1$  and  $\omega_2$ . The temperatures at both sides are fixed at  $T_h$  and  $T_c$ , respectively, with  $T_h > T_c$ . In this simple model, two resonators have internal absorption loss rates  $\gamma_{1,2}^i$  and in thermal equilibrium with the cold side at temperature

$T_c$ . The resonators also have coupling rates  $\gamma_{1,2}^e$  to the hot side at temperature  $T_h$ . In the ideal case, radiative coupling of mode 1 to the high-temperature side ( $\gamma_1^e$ ) and the internal loss of mode 2 ( $\gamma_2^i$ ) are both assumed to be zero. Therefore, when the ideal system is unmodulated, thermal emission from and absorption by the cold side are both zero and no net cooling or heating effect exists. When the system is modulated at a frequency  $\Omega = \omega_2 - \omega_1$ , a proportion of energy in mode 1 is up-converted to mode 2 and emitted to the hot side ( $P_{out}$ ), indicating a thermal photon-based cooling process. Simultaneously, a proportion of mode energy in mode 2 is down-converted to mode 1 and absorbed by the cold side ( $P_{in}$ ), indicating a thermal photon-based heating process. Although the rate of up- and down-conversion is equal for a single thermal photon, the number of thermally populated photons is unequal for both conversions which leads to a net cooling (or heating) effect. The net cooling power is determined as the difference between ( $P_{out} - P_{in}$ ) and the work done by the time modulation, a high thermodynamic performance approaching the Carnot limit of  $T_c/(T_h - T_c)$  is also accessible. The proposed mechanism is further numerically verified by using a physical structure

like defected one-dimensional photonic crystals. While the modulation format used in Buddhiraju’s work does not break reciprocity, it would be of interest to explore the consequence of reciprocity-breaking modulations for the construction of photon heat engines.

Here we make several remarks. First, Lorentz reciprocity can also be broken by optical nonlinearity [156–158]. Thermal radiation from nonlinear medium has been recently investigated [159–162]. However, the existing literature has not discussed the nonreciprocal effects of thermal radiation induced by nonlinearity. A rigorous analysis of these effects requires the formalism of nonlinear fluctuational electrodynamics [159], which is still under active development. It would be of interest to explore the consequences of nonlinearity for the construction of nonreciprocal thermal emitters.

Second, it is known that phase-change materials can be used to the effect of thermal rectification, which is also sometimes referred to as the effect of thermal diode [163–166]. However, this effect is fundamentally different from the nonreciprocal effects as discussed above: The thermal rectification effect is based on the temperature-dependent dielectric properties of the materials; it does not break Lorentz reciprocity. Consequently, Kirchhoff’s law stays valid; the angular spectral absorptivity and emissivity of a phase-change medium are equal, provided that these two quantities are measured under the same conditions (same temperatures, surrounding bodies, etc.).

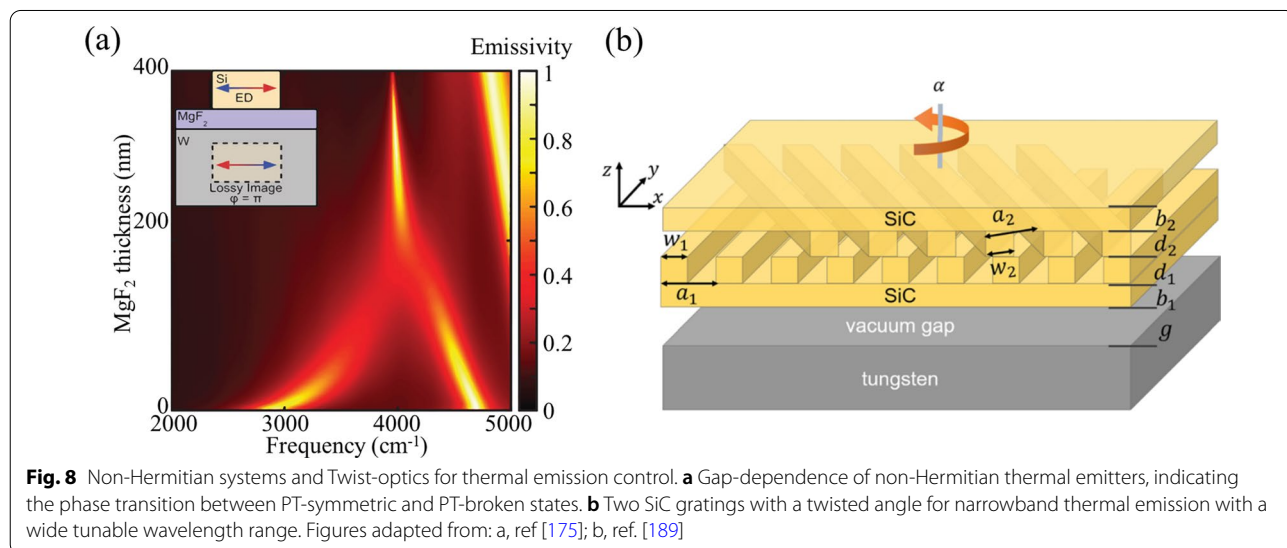
### 5 Summary and outlook

In summary, we overviewed engineered nanophotonic structures with broken symmetries in thermal photonics, mainly concentrating on the control of thermal emission.

Distinct from conventional materials and nanophotonic structures with high symmetries, broken geometrical symmetries including anisotropy, aperiodicity, randomness, and chirality are firstly discussed, highlighting the geometrical asymmetry-induced control of thermal emission and other thermal effects. Then, with engineered mode symmetries, peculiar nanophotonic states including Fano resonance and bound states in the continuum are also feasible for thermal emission control, enabling such as narrowband emission and complete switching of thermal emission. Lastly, by exploiting the magneto-optical effect and spatiotemporal modulation, the nonreciprocal thermal emission can violate Kirchhoff’s law. For future development, introducing more compound broken symmetries [10] and exploring the asymmetries in light-matter interactions [165] may bring new research opportunities. Additionally, we briefly discussed a few emerging directions: non-Hermitian system and twist-optics.

#### 5.1 Non-Hermiticity

In open quantum systems, the introduction of non-Hermiticity may bring profound results besides broadening resonances and decaying eigenstates [167, 168]. In particular, when a non-Hermitian system possesses a parity-time (PT) symmetry, real eigenvalues can appear in the non-Hermitian system and two or more eigenmodes can coalesce at an exceptional point [169]. Recently, various interesting applications are based on phase transition in non-Hermitian photonic systems at their exceptional points [167, 168, 170], including enhanced mode splitting [171, 172], topological energy transfer [173], and PT-symmetric lasing [174]. For thermal photonics, all thermal emitters are non-Hermitian systems, due to their



energy exchange with the environment. In Fig. 8a, Doiron et al. proposed and experimentally demonstrated non-Hermitian selective thermal emitters which exhibit the phase transition from passive PT-symmetric to broken PT-symmetric phase [175]. Using semiconductor–metal (Si–W) based thermal emitters, the coupling strength between a lossless Si resonator and a lossy W resonator is controlled by the spacer thickness. In the strong coupling regime (thin spacer), the two thermal emission branches show relatively broad emission peaks with small Q-factors. In the weak coupling regime (thick spacer), the two emission branches merge at the exceptional point resulting in a narrow emission peak with an enlarged Q-factor. Such non-Hermitian systems with passive PT-symmetry provide a novel approach to engineering selective thermal emitters. Additionally, with the combination of nonreciprocity and non-Hermiticity, Liu et al. proposed a MO-ENZ slab-based nonreciprocal thermal emitter [176]. When the loss is introduced in ENZ slabs, BICs and the corresponding topological phase singularity pairs (TPSPs) are separated due to the dispersion surface shifting along the imaginary axis. TPSPs possess topological robustness due to the topological charge conservation of BICs. When nonreciprocity is also introduced, asymmetric TPSPs occur in the angular space, leading to a near-complete violation of Kirchhoff's law of thermal radiation.

## 5.2 Twist-optics

Twistronics is an emerging research area that exhibits superior performance in manipulating optoelectronic properties. For 2D layered materials, the introduction of interlayer twist angle reconfigures the space group and electronic wave functions, more importantly, the breaking inversion and mirror symmetries lead to many interesting physical phenomena such as highly tunable optical nonlinearity [177–179], ferroelectricity [180, 181], and interlayer excitons [182]. As a photonic analog of twisted 2D layered materials, twisted anisotropic slabs and photonic crystals also provide new platforms to flexibly tune dispersion relation [183], engineered diffraction [184, 185], wavepacket localization [186, 187], and photonic flatbands [188]. Similarly, twisted photonic structures enable a highly desirable tunability in thermal photonics. As shown in Fig. 8b, Guo et al. numerically proposed a bilayer grating-based narrow thermal emitter with a wide tunable wavelength range [189] thanks to the twist sensitivity. The narrowband and polarization-dependent thermal emission results from the guided-mode resonance in the SiC grating. The emission peak positions are dependent on the period of the grating. A thin vacuum gap between the grating and tungsten surface determines the critical coupling condition of thermal emission.

Moiré fringes with an enlarged period are formed when a twisted interlayer angle appears between two gratings. Note that the effective grating period is extremely sensitive to the twisted angle, leading to a wide tunable wavelength range which is promising for multiplexed non-dispersive infrared (NDIR) gas sensing applications. Twisted layered structures also enable large tunability in the near-field radiative transfer process. Peng et al. numerically proposed two twisted ferromagnetic insulator slabs for the control of the near-field thermal transfer coefficient, which can be used as a near-field thermal switch [190]. A large and nonmonotonic thermal switch ratio results from nonreciprocal surface magnon-polaritons modes and twist-induced anisotropy in magnetized ferromagnetic insulators.

### Author contributions

All authors read and approved the final manuscript.

### Funding

S.F. acknowledges the support of the US Department of Energy (grant no. DE-FG02-07ER46426). W.L. acknowledges the support of the National Natural Science Foundation of China (grant nos. 62134009, 62121005), Development Program of the Science and Technology of Jilin Province (20200802001GH).

### Availability of data and materials

Not applicable.

### Declarations

### Competing interests

The authors declare that they have no competing interests.

### Author details

<sup>1</sup>GPL Photonics Laboratory, State Key Laboratory of Applied Optics, Fine Mechanics and Physics, Changchun Institute of Optics, Chinese Academy of Sciences, Changchun 130033, China. <sup>2</sup>Department of Applied Physics, Stanford University, Stanford, CA 94305, USA. <sup>3</sup>Department of Electrical Engineering, Ginzton Laboratory, Stanford University, Stanford, CA 94305, USA.

Received: 1 August 2022 Revised: 2 September 2022 Accepted: 5 September 2022

Published online: 02 December 2022

### References

1. S. Fan, Thermal photonics and energy applications. *Joule* **1**, 264–273 (2017)
2. W. Li, S. Fan, Nanophotonic control of thermal radiation for energy applications [Invited]. *Opt. Express* **26**, 15995–16021 (2018)
3. D.G. Baranov et al., Nanophotonic engineering of far-field thermal emitters. *Nat. Mater.* **18**, 920–930 (2019)
4. J.C. Cuevas, F.J. García-Vidal, Radiative heat transfer. *ACS Photonics* **5**, 3896–3915 (2018)
5. S.A. Biehs et al., Near-field radiative heat transfer in many-body systems. *Rev. Mod. Phys.* **93**, 25009 (2021)
6. Y. Li et al., Transforming heat transfer with thermal metamaterials and devices. *Nat. Rev. Mater.* **6**, 488–507 (2021)
7. S. Fan, W. Li, Photonics and thermodynamics concepts in radiative cooling. *Nat. Photonics* **16**, 182–190 (2022)
8. Schwichtenberg, *J. Physics from symmetry*. (Springer, Cham, 2015).
9. C. Guo, Z. Zhao, S. Fan, Internal transformations and internal symmetries in linear photonic systems. *Phys. Rev. A* **105**, 023509 (2022)



10. C. Guo, B. Zhao, S. Fan, Adjoint Kirchhoff's law and general symmetry implications for all thermal emitters. *Phys. Rev. X* **12**, 121023 (2022)
11. X. Liu et al., Taming the blackbody with infrared metamaterials as selective thermal emitters. *Phys. Rev. Lett.* **107**, 45901 (2011)
12. M. De Zoysa et al., Conversion of broadband to narrowband thermal emission through energy recycling. *Nat. Photonics* **6**, 535–539 (2012)
13. J.A. Bossard et al., Near-ideal optical metamaterial absorbers with super-octave bandwidth. *ACS Nano* **8**, 1517–1524 (2014)
14. Y.X. Yeng et al., Enabling high-temperature nanophotonics for energy applications. *Proc. Natl. Acad. Sci.* **109**, 2280–2285 (2012)
15. J.A. Schuller, T. Taubner, M.L. Brongersma, Optical antenna thermal emitters. *Nat. Photonics* **3**, 658–661 (2009)
16. Y. Miyoshi et al., High-speed and on-chip graphene blackbody emitters for optical communications by remote heat transfer. *Nat. Commun.* **9**, 1279 (2018)
17. J. Li, B. Liu, S. Shen, Tunable narrow-band near-field thermal emitters based on resonant metamaterials. *Phys. Rev. B* **96**, 075413 (2017)
18. B. Liu, J. Li, S. Shen, Resonant thermal infrared emitters in near- and far-fields. *ACS Photonics* **4**, 1552–1557 (2017)
19. J.J. Greffet et al., Coherent emission of light by thermal sources. *Nature* **416**, 61–64 (2002)
20. S.E. Han, Theory of thermal emission from periodic structures. *Phys. Rev. B* **80**, 155108 (2009)
21. F. Marquier et al., Coherent spontaneous emission of light by thermal sources. *Phys. Rev. B* **69**, 155412 (2004)
22. K. Ito, T. Matsui, H. Iizuka, Thermal emission control by evanescent wave coupling between guided mode of resonant grating and surface phonon polariton on silicon carbide plate. *Appl. Phys. Lett.* **104**, 051127 (2014)
23. H. Chalabi, A. Alù, M.L. Brongersma, Focused thermal emission from a nanostructured SiC surface. *Phys. Rev. B* **94**, 094307 (2016)
24. M. Hu et al., Gold nanostructures: engineering their plasmonic properties for biomedical applications. *Chem. Soc. Rev.* **35**, 1084–1094 (2006)
25. A. Poddubny, I. Iorsh, P. Belov, Y. Kivshar, Hyperbolic metamaterials. *Nat. Photonics* **7**, 948–957 (2013)
26. L. Ferrari, C. Wu, D. Lepage, X. Zhang, Z. Liu, Hyperbolic metamaterials and their applications. *Prog. Quantum Electron.* **40**, 1–40 (2015)
27. W. Gao, C.F. Doiron, X. Li, J. Kono, G.V. Naik, Macroscopically aligned carbon nanotubes as a refractory platform for hyperbolic thermal emitters. *ACS Photonics* **6**, 1602–1609 (2019)
28. N. Komatsu et al., Modulation-doped multiple quantum wells of aligned single-wall carbon nanotubes. *Adv. Funct. Mater.* **27**, 1606022 (2017)
29. J.A. Roberts et al., Tunable hyperbolic metamaterials based on self-assembled carbon nanotubes. *Nano Lett.* **19**, 3131–3137 (2019)
30. M.G. Nielsen, A. Pors, O. Albrektsen, S.I. Bozhevolnyi, Efficient absorption of visible radiation by gap plasmon resonators. *Opt. Express* **20**, 13311–13319 (2012)
31. S. Pillai, M.A. Green, Plasmonics for photovoltaic applications. *Sol. Energy Mater. Sol. Cells* **94**, 1481–1486 (2010)
32. K. Aydin, V.E. Ferry, R.M. Briggs, H.A. Atwater, Broadband polarization-independent resonant light absorption using ultrathin plasmonic super absorbers. *Nat. Commun.* **2**, 517 (2011)
33. W. Li, J. Valentine, Metamaterial perfect absorber based hot electron photodetection. *Nano Lett.* **14**, 3510–3514 (2014)
34. T. Wang et al., Phonon-polaritonic bowtie nanoantennas: controlling infrared thermal radiation at the nanoscale. *ACS Photonics* **4**, 1753–1760 (2017)
35. Y. Cui et al., Ultrabroadband light absorption by a sawtooth anisotropic metamaterial slab. *Nano Lett.* **12**, 1443–1447 (2012)
36. H. Hu, D. Ji, X. Zeng, K. Liu, Q. Gan, Rainbow trapping in hyperbolic metamaterial waveguide. *Sci. Rep.* **3**, 1249 (2013)
37. Q. Liu et al., Non-tapered metamaterial emitters for radiative cooling to low temperature limit. *Opt. Commun.* **450**, 246–251 (2019)
38. S. Yu, C.W. Qiu, Y. Chong, S. Torquato, N. Park, Engineered disorder in photonics. *Nat. Rev. Mater.* **6**, 226–243 (2021)
39. D.S. Wiersma, Disordered photonics. *Nat. Photonics* **7**, 188–196 (2013)
40. A.P. Raman, M.A. Anoma, L. Zhu, E. Rephaeli, S. Fan, Passive radiative cooling below ambient air temperature under direct sunlight. *Nature* **515**, 540–544 (2014)
41. W. Zhang, B. Wang, C. Zhao, Selective thermophotovoltaic emitter with aperiodic multilayer structures designed by machine learning. *ACS Appl. Energy Mater.* **4**, 2004–2013 (2021)
42. A. Sakurai et al., Ultranarrow-band wavelength-selective thermal emission with aperiodic multilayered metamaterials designed by bayesian optimization. *ACS Cent. Sci.* **5**, 319–326 (2019)
43. C. Dong et al., Quasiperiodic metamaterials empowered non-metallic broadband optical absorbers. *Opt. Express* **29**, 13576–13589 (2021)
44. M.E. Zoorob, M.D.B. Charlton, G.J. Parker, J.J. Baumberg, M.C. Netti, Complete photonic bandgaps in 12-fold symmetric quasicrystals. *Nature* **404**, 740–743 (2000)
45. Z.V. Vardeny, A. Nahata, A. Agrawal, Optics of photonic quasicrystals. *Nat. Photonics* **7**, 177–187 (2013)
46. W. Man, M. Megens, P.J. Steinhart, P.M. Chaikin, Experimental measurement of the photonic properties of icosahedral quasicrystals. *Nature* **436**, 993–996 (2005)
47. J. Xavier et al., Quasicrystalline-structured light harvesting nanophotonic silicon films on nanoimprinted glass for ultra-thin photovoltaics. *Opt. Mater. Express* **4**, 2290–2299 (2014)
48. C. Bauer, H. Giessen, Light harvesting enhancement in solar cells with quasicrystalline plasmonic structures. *Opt. Express* **21**, A363–A371 (2013)
49. T.M. Mercier et al., High symmetry nano-photonics quasi-crystals providing novel light management in silicon solar cells. *Nano Energy* **84**, 105874 (2021)
50. J.H. Park, S.E. Han, P. Nagpal, D.J. Norris, Observation of thermal beaming from tungsten and molybdenum Bull's eyes. *ACS Photonics* **3**, 494–500 (2016)
51. O. Ilic et al., Tailoring high-temperature radiation and the resurrection of the incandescent source. *Nat. Nanotechnol.* **11**, 320–324 (2016)
52. B. Zhu et al., Subambient daytime radiative cooling textile based on nanoprocessed silk. *Nat. Nanotechnol.* **16**, 1342–1348 (2021)
53. Y. Zhai et al., Scalable-manufactured randomized glass-polymer hybrid metamaterial for daytime radiative cooling. *Science* **355**, 1062–1066 (2017)
54. M. Hentschel, M. Schäferling, X. Duan, H. Giessen, N. Liu, Chiral plasmonics. *Sci. Adv.* **3**, e1602735 (2017)
55. Y. Chen et al., Multidimensional nanoscopic chiroptics. *Nat. Rev. Phys.* **4**, 113–124 (2022)
56. Y. Tang, A.E. Cohen, Enhanced enantioselectivity in excitation of chiral molecules by superchiral light. *Science* **332**, 333–336 (2011)
57. Y. Tang, A.E. Cohen, Optical chirality and its interaction with matter. *Phys. Rev. Lett.* **104**, 163901 (2010)
58. E. Mohammadi et al., Accessible superchiral near-fields driven by tailored electric and magnetic resonances in all-dielectric nanostructures. *ACS Photonics* **6**, 1939–1946 (2019)
59. M. Schäferling, D. Dregely, M. Hentschel, H. Giessen, Tailoring enhanced optical chirality: design principles for chiral plasmonic nanostructures. *Phys. Rev. X* **2**, 031010 (2012)
60. W. Li et al., Circularly polarized light detection with hot electrons in chiral plasmonic metamaterials. *Nat. Commun.* **6**, 8379 (2015)
61. T. Liu et al., Chiral plasmonic nanocrystals for generation of hot electrons: toward polarization-sensitive photochemistry. *Nano Lett.* **19**, 1395–1407 (2019)
62. W. Wang et al., Generation of hot electrons with chiral metamaterial perfect absorbers: giant optical chirality for polarization-sensitive photochemistry. *ACS Photonics* **6**, 3241–3252 (2019)
63. A. Rafiei Miandashti, L. Khosravi Khorashad, M.E. Kordesch, A.O. Govorov, H.H. Richardson, Experimental and theoretical observation of photothermal chirality in gold nanoparticle helicoids. *ACS Nano* **14**, 4188–4195 (2020)
64. X.T. Kong, L. Khosravi Khorashad, Z. Wang, A.O. Govorov, Photothermal circular dichroism induced by plasmon resonances in chiral metamaterial absorbers and bolometers. *Nano Lett.* **18**, 2001–2008 (2018)
65. S.L. Wadsworth, P.G. Clem, E.D. Branson, G.D. Boreman, Broadband circularly-polarized infrared emission from multilayer metamaterials. *Opt. Mater. Express* **1**, 466–479 (2011)
66. J. Ginn, D. Shelton, P. Krenz, B. Lail, G. Boreman, Polarized infrared emission using frequency selective surfaces. *Opt. Express* **18**, 4557–4563 (2010)

67. C. Wu et al., Spectrally selective chiral silicon metasurfaces based on infrared Fano resonances. *Nat. Commun.* **5**, 3892 (2014)
68. N. Dahan, Y. Gorodetski, K. Frischwasser, V. Kleiner, E. Hasman, Geometric Doppler effect: Spin-split dispersion of thermal radiation. *Phys. Rev. Lett.* **105**, 136402 (2010)
69. K. Frischwasser, I. Yulevich, V. Kleiner, E. Hasman, Rashba-like spin degeneracy breaking in coupled thermal antenna lattices. *Opt. Express* **19**, 23475–23482 (2011)
70. N. Shitrit et al., Spin-Optical metamaterial route to spin-controlled photonics. *Science* **340**, 724–726 (2013)
71. P. Spaeth et al., Circular dichroism measurement of single metal nanoparticles using photothermal imaging. *Nano Lett.* **19**, 8934–8940 (2019)
72. X. Lan et al., DNA-guided plasmonic helix with switchable chirality. *J. Am. Chem. Soc.* **140**, 11763–11770 (2018)
73. M. Selmke, M. Braun, F. Cichos, Photothermal single-particle microscopy: Detection of a nanolens. *ACS Nano* **6**, 2741–2749 (2012)
74. A.C. Overvig, S.A. Mann, A. Alù, Thermal metasurfaces: complete emission control by combining local and nonlocal light-matter interactions. *Phys. Rev. X* **11**, 21050 (2021)
75. A.C. Overvig, S.C. Malek, N. Yu, Multifunctional nonlocal metasurfaces. *Phys. Rev. Lett.* **125**, 17402 (2020)
76. A. Overvig, A. Alù, Wavefront-selective Fano resonant metasurfaces. *Adv. Photonics* **3**, 026002 (2021)
77. Wang, X. et al. Observation of non-vanishing optical helicity in thermal radiation from symmetry-broken metasurfaces. *arXiv Prepr.* 2205.05926 (2022).
78. C. Khandekar, Z. Jacob, Circularly polarized thermal radiation from nonequilibrium coupled antennas. *Phys. Rev. Appl.* **12**, 014053 (2019)
79. M. Holub, P. Bhattacharya, Spin-polarized light-emitting diodes and lasers. *J. Phys. D: Appl. Phys.* **40**, R179 (2007)
80. S. Fan, J.D. Joannopoulos, Analysis of guided resonances in photonic crystal slabs. *Phys. Rev. B* **65**, 235112 (2002)
81. S. Fan, W. Suh, J.D. Joannopoulos, Temporal coupled-mode theory for the Fano resonance in optical resonators. *J. Opt. Soc. Am. A* **20**, 569–572 (2003)
82. A.E. Miroshnichenko, S. Flach, Y.S. Kivshar, Fano resonances in nanoscale structures. *Rev. Mod. Phys.* **82**, 2257–2298 (2010)
83. M.F. Limonov, M.V. Rybin, A.N. Poddubny, Y.S. Kivshar, Fano resonances in photonics. *Nat. Photonics* **11**, 543–554 (2017)
84. B. Luk'Yanchuk et al., The Fano resonance in plasmonic nanostructures and metamaterials. *Nat. Mater.* **9**, 707–715 (2010)
85. L. Stern, M. Grajower, U. Levy, Fano resonances and all-optical switching in a resonantly coupled plasmonic-atomic system. *Nat. Commun.* **5**, 4865 (2014)
86. K. Nozaki et al., Ultralow-energy and high-contrast all-optical switch involving Fano resonance based on coupled photonic crystal nanocavities. *Opt. Express* **21**, 11877–11888 (2013)
87. G. Dong, Y. Wang, X. Zhang, High-contrast and low-power all-optical switch using Fano resonance based on a silicon nanobeam cavity. *Opt. Lett.* **43**, 5977–5980 (2018)
88. S. Fan, Sharp asymmetric line shapes in side-coupled waveguide-cavity systems. *Appl. Phys. Lett.* **80**, 908–910 (2002)
89. M. ElKabbash et al., Fano-resonant ultrathin film optical coatings. *Nat. Nanotechnol.* **16**, 440–446 (2021)
90. D. Kraemer et al., High-performance flat-panel solar thermoelectric generators with high thermal concentration. *Nat. Mater.* **10**, 532–538 (2011)
91. X. Zhang, Z.G. Zhang, Q. Wang, S.N. Zhu, H. Liu, Controlling thermal emission by parity-symmetric Fano resonance of optical absorbers in metasurfaces. *ACS Photonics* **6**, 2671–2676 (2019)
92. J.E. Pérez-Rodríguez, G. Pirruccio, R. Esquivel-Sirvent, Fano interference for tailoring near-field radiative heat transfer. *Phys. Rev. Mater.* **1**, 062201 (2017)
93. C.W. Hsu et al., Observation of trapped light within the radiation continuum. *Nature* **499**, 188–191 (2013)
94. C.W. Hsu, B. Zhen, A.D. Stone, J.D. Joannopoulos, M. Soljac, Bound states in the continuum. *Nat. Rev. Mater.* **1**, 16048 (2016)
95. T. Ochiai, K. Sakoda, Dispersion relation and optical transmittance of a hexagonal photonic crystal slab. *Phys. Rev. B* **63**, 125107 (2001)
96. Y. Plotnik et al., Experimental observation of optical bound states in the continuum. *Phys. Rev. Lett.* **107**, 183901 (2011)
97. J. Lee et al., Observation and differentiation of unique high-Q optical resonances near zero wave vector in macroscopic photonic crystal slabs. *Phys. Rev. Lett.* **109**, 67401 (2012)
98. Y. Yang, C. Peng, Y. Liang, Z. Li, S. Noda, Analytical perspective for bound states in the continuum in photonic crystal slabs. *Phys. Rev. Lett.* **113**, 37401 (2014)
99. M. Liu, D.Y. Choi, Extreme Huygens' metasurfaces based on quasi-bound states in the continuum. *Nano Lett.* **18**, 8062–8069 (2018)
100. Z. Sakotic, A. Krasnok, N. Cselyusza, N. Jankovic, A. Alù, Berreman embedded eigenstates for narrow-band absorption and thermal emission. *Phys. Rev. Appl.* **13**, 064073 (2020)
101. M.G. Silveirinha, Trapping light in open plasmonic nanostructures. *Phys. Rev. A* **89**, 023813 (2014)
102. F. Monticone, A. Alu, Embedded photonic eigenvalues in 3D nanostructures. *Phys. Rev. Lett.* **112**, 213903 (2014)
103. L. Li, J. Zhang, C. Wang, N. Zheng, H. Yin, Optical bound states in the continuum in a single slab with zero refractive index. *Phys. Rev. A* **96**, 013801 (2017)
104. Z. Sakotic, A. Krasnok, A. Alù, N. Jankovic, Topological scattering singularities and embedded eigenstates for polarization control and sensing applications. *Photonics Res.* **9**, 1310 (2021)
105. F. Monticone, H.M. Doeleman, W. Den Hollander, A.F. Koenderink, A. Alù, Trapping light in plain sight: embedded photonic eigenstates in zero-index metamaterials. *Laser Photonics Rev.* **12**, 1700220 (2018)
106. S.I. Azzam, A.V. Kildishev, Photonic bound states in the continuum: from basics to applications. *Adv. Opt. Mater.* **9**, 16–24 (2021)
107. K. Koshelev, S. Lepeshov, M. Liu, A. Bogdanov, Y. Kivshar, Asymmetric metasurfaces with High-Q resonances governed by bound states in the continuum. *Phys. Rev. Lett.* **121**, 193903 (2018)
108. A.A. Bogdanov et al., Bound states in the continuum and Fano resonances in the strong mode coupling regime. *Adv. Photonics* **1**, 016001 (2019)
109. J. Tian et al., High-Q all-dielectric metasurface: super and suppressed optical absorption. *ACS Photonics* **7**, 1436–1443 (2020)
110. J. Yu et al., Dielectric super-absorbing metasurfaces via PT symmetry breaking. *Optica* **8**, 1290–1295 (2021)
111. Haus, H. *Waves and fields in optoelectronics*. (PRENTICE-HALL, INC., 1984).
112. C. Guo, S. Fan, Reciprocity constraints on reflection. *Phys. Rev. Lett.* **128**, 256101 (2022)
113. J.J. Greffet, P. Bouchon, G. Brucoli, F. Marquier, Light emission by non-equilibrium bodies: local Kirchhoff Law. *Phys. Rev. X* **8**, 21008 (2018)
114. L. Zhu, S. Fan, Near-complete violation of detailed balance in thermal radiation. *Phys. Rev. B* **90**, 220301 (2014)
115. H. Ries, Complete and reversible absorption of radiation. *Appl. Phys. B* **32**, 153–156 (1983)
116. M.A. Green, Time-asymmetric photovoltaics. *Nano Lett.* **12**, 5985–5988 (2012)
117. Y. Park, B. Zhao, S. Fan, Reaching the ultimate efficiency of solar energy harvesting with a nonreciprocal multijunction solar cell. *Nano Lett.* **22**, 448–452 (2022)
118. Green, M. A. *Third Generation Photovoltaics: Advanced Solar Energy Conversion*. (Springer-Verlag, Berlin, 2003).
119. L. Bi, Materials for nonreciprocal photonics. *MRS Bull.* **43**, 408–412 (2018)
120. L. Bi et al., On-chip optical isolation in monolithically integrated non-reciprocal optical resonators. *Nat. Photonics* **5**, 758–762 (2011)
121. D.A.B. Miller, L. Zhu, S. Fan, Universal modal radiation laws for all thermal emitters. *Proc. Natl. Acad. Sci. U. S. A.* **114**, 4336–4341 (2017)
122. Y. Park et al., Violating Kirchhoff's Law of thermal radiation in semitransparent structures. *ACS Photonics* **8**, 2417–2424 (2021)
123. K. Shayegan, B. Zhao, Y. Kim, S. Fan, H. Atwater, Nonreciprocal infrared absorption via resonant magneto-optical coupling to InAs. *Sci. Adv.* **8**, eabm4308 (2022)
124. B. Zhao et al., Near-complete violation of Kirchhoff's law of thermal radiation with a 0.3 T magnetic field. *Opt. Lett.* **44**, 4203–4206 (2019)
125. T. Liu, N. Kobayashi, K. Ikeda, Y. Ota, S. Iwamoto, Topological band gaps enlarged in Epsilon-Near-Zero magneto-optical photonic crystals. *ACS Photonics* **9**, 1621–1626 (2021)
126. G. Armelles, A. Cebollada, A. García-Martín, M.U. González, Magneto-plasmonics: combining magnetic and plasmonic functionalities. *Adv. Opt. Mater.* **1**, 10–35 (2013)

127. Z. Tan, F. Fan, X. Dong, J. Cheng, S. Chang, Nonreciprocal terahertz beam steering based on magneto-optic metagratings. *Sci. Rep.* **9**, 20210 (2019)
128. Liu, M. et al. Nonreciprocal thermal radiation in ultrathin magnetized epsilon-near-zero semiconductors. *arXiv Prepr.* 2203.04488 (2022).
129. C. Guo, B. Zhao, D. Huang, S. Fan, Radiative thermal router based on tunable magnetic Weyl semimetals. *ACS Photonics* **7**, 3257–3263 (2020)
130. Y. Tsurimaki et al., Large nonreciprocal absorption and emission of radiation in type-I Weyl semimetals with time reversal symmetry breaking. *Phys. Rev. B* **101**, 165426 (2020)
131. S. Pajovic, Y. Tsurimaki, X. Qian, G. Chen, Intrinsic nonreciprocal reflection and violation of Kirchhoff's law of radiation in planar type-I magnetic Weyl semimetal surfaces. *Phys. Rev. B* **102**, 165417 (2020)
132. B. Zhao, C. Guo, C.A.C. Garcia, P. Narang, S. Fan, Axion-field-enabled nonreciprocal thermal radiation in Weyl semimetals. *Nano Lett.* **20**, 1923–1927 (2020)
133. V.S. Asadchy, C. Guo, B. Zhao, S. Fan, Sub-wavelength passive optical isolators using photonic structures based on Weyl semimetals. *Adv. Opt. Mater.* **8**, 36–39 (2020)
134. Y. Wang et al., Broadband circularly polarized thermal radiation from magnetic Weyl semimetals. *Opt. Mater. Express* **11**, 3880–3895 (2021)
135. L. Zhu, S. Fan, Persistent directional current at equilibrium in nonreciprocal many-body near field electromagnetic heat transfer. *Phys. Rev. Lett.* **117**, 134303 (2016)
136. L. Zhu, Y. Guo, S. Fan, Theory of many-body radiative heat transfer without the constraint of reciprocity. *Phys. Rev. B* **97**, 094302 (2018)
137. S. Buddhiraju, P. Santhanam, S. Fan, Thermodynamic limits of energy harvesting from outgoing thermal radiation. *Proc. Natl. Acad. Sci. U. S. A.* **115**, E3609–E3615 (2018)
138. A. Ott, S.A. Biehs, P. Ben-Abdallah, Anomalous photon thermal Hall effect. *Phys. Rev. B* **101**, 241411 (2020)
139. C. Guo, Y. Guo, S. Fan, Relation between photon thermal Hall effect and persistent heat current in nonreciprocal radiative heat transfer. *Phys. Rev. B* **100**, 205416 (2019)
140. C. Guo, S. Fan, Theoretical constraints on reciprocal and non-reciprocal many-body radiative heat transfer. *Phys. Rev. B* **102**, 085401 (2020)
141. P. Ben-Abdallah, Photon thermal hall effect. *Phys. Rev. Lett.* **116**, 084301 (2016)
142. Z. Yu, S. Fan, Complete optical isolation created by indirect interband photonic transitions. *Nat. Photonics* **3**, 91–94 (2009)
143. C. Caloz et al., Electromagnetic Nonreciprocity. *Phys. Rev. Appl.* **10**, 047001 (2018)
144. M.C. Rechtsman et al., Photonic Floquet topological insulators. *Nature* **496**, 196–200 (2013)
145. I. Williamson et al., Integrated nonreciprocal photonic devices with dynamic modulation. *Proc. IEEE* **108**, 1759–1784 (2020)
146. S. Yin, E. Galiffi, A. Alù, Floquet metamaterials. *eLight* **2**, 8 (2022)
147. D.L. Sounas, C. Caloz, A. Alù, Giant non-reciprocity at the subwavelength scale using angular momentum-biased metamaterials. *Nat. Commun.* **4**, 2407 (2013)
148. D.L. Sounas, A. Alù, Non-reciprocal photonics based on time modulation. *Nat. Photonics* **11**, 774–783 (2017)
149. K. Fang, Z. Yu, S. Fan, Photonic Aharonov-Bohm effect based on dynamic modulation. *Phys. Rev. Lett.* **108**, 153901 (2012)
150. Y. Hadad, J.C. Soric, A. Alu, Breaking temporal symmetries for emission and absorption. *Proc. Natl. Acad. Sci. U. S. A.* **113**, 3471–3475 (2016)
151. A. Ghanekar, J. Wang, S. Fan, M.L. Povinelli, Violation of Kirchhoff's Law of Thermal Radiation with Space-Time Modulated Grating. *ACS Photonics* **9**, 1157–1164 (2022)
152. L.J. Fernández-Alcázar, R. Kononchuk, H. Li, T. Kottos, Extreme nonreciprocal near-field thermal radiation via floquet photonics. *Phys. Rev. Lett.* **126**, 204101 (2021)
153. H. Li, B. Shapiro, T. Kottos, Floquet scattering theory based on effective Hamiltonians of driven systems. *Phys. Rev. B* **98**, 121101 (2018)
154. H. Li, T. Kottos, B. Shapiro, Floquet-network theory of nonreciprocal transport. *Phys. Rev. Appl.* **9**, 44031 (2018)
155. S. Buddhiraju, W. Li, S. Fan, Photonic refrigeration from time-modulated thermal emission. *Phys. Rev. Lett.* **124**, 77402 (2020)
156. Y. Shi, Z. Yu, S. Fan, Limitations of nonlinear optical isolators due to dynamic reciprocity. *Nat. Photonics* **9**, 388–392 (2015)
157. L. Fan et al., An all-silicon passive optical diode. *Science* **335**, 447–450 (2012)
158. T. Shui, W.-X. Yang, M.-T. Cheng, R.-K. Lee, Optical nonreciprocity and nonreciprocal photonic devices with directional four-wave mixing effect. *Opt. Express* **30**, 6284–6299 (2022)
159. H. Soo, M. Krüger, Fluctuational electrodynamics for nonlinear media. *EPL* **115**, 41002 (2016)
160. C. Khandekar, A. Pick, S.G. Johnson, A.W. Rodriguez, Radiative heat transfer in nonlinear Kerr media. *Phys. Rev. B* **91**, 115406 (2015)
161. C. Khandekar, A.W. Rodriguez, Near-field thermal upconversion and energy transfer through a Kerr medium. *Opt. Express* **25**, 23164–23180 (2017)
162. C. Khandekar, R. Messina, A.W. Rodriguez, Near-field refrigeration and tunable heat exchange through four-wave mixing. *AIP Adv.* **8**, 055029 (2018)
163. C.R. Otey, W.T. Lau, S. Fan, Thermal rectification through vacuum. *Phys. Rev. Lett.* **104**, 154301 (2010)
164. P. Ben-Abdallah, S.A. Biehs, Phase-change radiative thermal diode. *Appl. Phys. Lett.* **103**, 191907 (2013)
165. A. Fiorino et al., A thermal diode based on nanoscale thermal radiation. *ACS Nano* **12**, 5174–5179 (2018)
166. A. Ghanekar, J. Ji, Y. Zheng, High-rectification near-field thermal diode using phase change periodic nanostructure. *Appl. Phys. Lett.* **109**, 123106 (2016)
167. L. Feng, R. El-Ganainy, L. Ge, Non-Hermitian photonics based on parity-time symmetry. *Nat. Photonics* **11**, 752–762 (2017)
168. R. El-Ganainy et al., Non-Hermitian physics and PT symmetry. *Nat. Phys.* **14**, 11–19 (2018)
169. C.M. Bender, S. Boettcher, Real spectra in non-hermitian hamiltonians having PT symmetry. *Phys. Rev. Lett.* **80**, 5243–5246 (1998)
170. M.A. Miri, A. Alù, Exceptional points in optics and photonics. *Science* **363**, eaar7709 (2019)
171. Z.P. Liu et al., Metrology with PT-symmetric cavities: enhanced sensitivity near the PT-phase transition. *Phys. Rev. Lett.* **117**, 110802 (2016)
172. W. Chen, Ş.K. Özdemir, G. Zhao, J. Wiersig, L. Yang, Exceptional points enhance sensing in an optical microcavity. *Nature* **548**, 192–195 (2017)
173. J. Doppler et al., Dynamically encircling an exceptional point for asymmetric mode switching. *Nature* **537**, 76–79 (2016)
174. H. Hossein, M. Mohammad-Ali, H. Matthias, K. Mercedeh, Parity-time-symmetric microring lasers. *Science* **346**, 975–978 (2014)
175. C.F. Doiron, G.V. Naik, Non-Hermitian selective thermal emitters using metal-semiconductor hybrid resonators. *Adv. Mater.* **31**, 1904154 (2019)
176. M. Liu et al., Evolution and nonreciprocity of loss-induced topological phase singularity pairs. *Phys. Rev. Lett.* **127**, 266101 (2021)
177. W.T. Hsu et al., Second harmonic generation from artificially stacked transition metal dichalcogenide twisted bilayers. *ACS Nano* **8**, 2951–2958 (2014)
178. C.J. Kim et al., Stacking order dependent second harmonic generation and topological defects in h-BN bilayers. *Nano Lett.* **13**, 5660–5665 (2013)
179. A. Autere et al., Nonlinear Optics with 2D layered materials. *Adv. Mater.* **30**, 1705963 (2018)
180. K. Yasuda, X. Wang, K. Watanabe, T. Taniguchi, P. Jarillo-Herrero, Stacking-engineered ferroelectricity in bilayer boron nitride. *Science* **372**, 1458–1462 (2021)
181. M.V. Stern et al., Interfacial ferroelectricity by van der Waals sliding. *Science* **372**, 1462–1466 (2021)
182. T. Jiang et al., Valley and band structure engineering of folded MoS<sub>2</sub> bilayers. *Nat. Nanotechnol.* **9**, 825–829 (2014)
183. G. Hu et al., Topological polaritons and photonic magic angles in twisted α-MoO<sub>3</sub> bilayers. *Nature* **582**, 209–213 (2020)
184. B. Lou et al., Theory for twisted bilayer photonic crystal slabs. *Phys. Rev. Lett.* **126**, 136101 (2021)
185. B. Lou, S. Fan, Tunable frequency filter based on twisted bilayer photonic crystal slabs. *ACS Photonics* **9**, 800–805 (2022)
186. Q. Fu et al., Optical soliton formation controlled by angle twisting in photonic moiré lattices. *Nat. Photonics* **14**, 663–668 (2020)

187. P. Wang et al., Localization and delocalization of light in photonic moiré lattices. *Nature* **577**, 42–46 (2020)
188. H. Tang et al., Modeling the optical properties of twisted bilayer photonic crystals. *Light Sci. Appl.* **10**, 157 (2021)
189. C. Guo, Y. Guo, B. Lou, S. Fan, Wide wavelength-tunable narrow-band thermal radiation from moiré patterns. *Appl. Phys. Lett.* **118**, 131111 (2021)
190. J. Peng et al., Twist-induced near-field thermal switch using nonreciprocal surface magnon-polaritons. *ACS Photonics* **8**, 2183–2189 (2021)